Brandenburgische Technische Universität Cottbus-Senftenberg

MASTER THESIS

Utilizing Satellite Data to Assess the Impacts of Floods

Author:

Aysha Akter

Supervisors:

Prof. Dr. rer. nat. Christoph Hinz

and

Jeremy Nicolas Eudaric

A thesis submitted in fulfillment of the requirements

for the degree of

Master of Science

from the faculty of

Environment and Natural Sciences

in

Environmental and Resource Management

Deutsches Zentrum für Luft- und Raumfahrt

Brandenburg University of Technology Cottbus - Senftenberg

Declaration of Authorship

I, Aysha Akter, declare that this thesis titled: "Utilizing Satellite Data to Assess the Impacts of Floods" and the work presented in it are my own. I confirm that:

- The work in this thesis is my own, and all the data analysis, interpretation, and conclusions were carried out by me.
- This work has been done in collaboration with Deutsches Zentrum für Luft- und Raumfahrt (German Aerospace Center, DLR).
- This work was done wholly or mainly while I was pursuing a research degree at this university.
- Source of information, data, or ideas taken from other authors, publications, or online has been properly acknowledged and cited.
  This thesis has not been handed in or published before in the same or similar form.
- I have acknowledged all the main sources of help.
- I have published all the codes on my GitHub [1] account, and it is public to all.

Cottbus, June 18th, 2026



Aysha Akter

1 Github repository link: https://github.com/ayshaa786/flood_risk_index.

All codes are written in Jupyter Notebook.

Abstract

Floods are one of the most common and devastating disasters among natural hazards, impacting millions of people each year and resulting in significant damage to infrastructure, agriculture and livelihoods. In developing countries such as Pakistan, the frequency of floods is increasing, population is growing fast, urban expansion, and socio-economic inequalities contribute further to exacerbate disaster risk in this country. The objective is to assess flood risk by using satellite imagery to detect flood hazards, produce rapid flood maps, and combine these outputs with geospatial, subnational exposure, and socioeconomic data to evaluate potential impacts and vulnerabilities.

The framework was employed to 36 municipalities in the northern part of Sindh Province, Pakistan, with two flood event scenarios for the years 2020 and 2025. Flood hazard was generated from Sentinel-1 SAR imagery and was validated with optical imagery.

The outcomes indicate that flood risk is different around the study area. In 2020, the most vulnerable municipalities were located in the western and central regions of the northern part of Sindh, including Dadu, Thul, Sehwan, Kandhkot, Tangwani, Gambat, Khairpur, Dokri, Ratodero, Nasirabad, Shahdad Kot, and Sijawal Junejo. By 2025, the risk of flooding was moving towards the eastern municipalities, particularly towards Khanpur, Pano Aqil, and Khairpur. The results showed that exposure greatly contributed to the increase in flood risk observed during the study period, especially a higher population and building densities, whereas the vulnerability was fairly constant during the study. Generally, municipalities with higher poverty rates, lower human development, and higher socio-economic inequality had higher vulnerability and lower adaptive capacity.

The generated framework (Flood Risk Index) could be used to prioritize municipalities for disaster management planning, emergency response strategies, and resource allocation by identifying the municipalities that are at risk. Moreover, the framework helps achieve Sustainable Development Goal (SDG) 11 (sustainable cities and communities), of making cities resilient and adopting measures to prevent disasters, as well as SDG 13 (Climate Action) of climate action and making decisions on the basis of risks. The use of readily available data and the steps taken here are easily replicable, making the framework suitable for implementation in other highly vulnerable areas of the world where data is limited.

Acknowledgement

I would like to express my sincere gratitude and heartfelt thanks to Jeremy Nicolas Eudaric, who gave me the opportunity to do my Master's thesis under his supervision within the research group (AI4EO) at the Deutsches Zentrum für Luft- und Raumfahrt (German Aerospace Center, DLR). Throughout the course of my thesis, his constant guidance, helpful suggestions, constructive feedback, and encouragement were priceless. He was always there when I needed him, and he gave me great, insightful discussions, which helped me to complete this thesis successfully.

In Addition, I would like to express my gratitude to Prof. Dr. Christoph Hinz, the academic supervisor of this work, at the Brandenburg University of Technology Cottbus-Senftenberg (BTU). He gave valuable scientific direction throughout this thesis process and his guidance, support, and valuable advice helped me to complete this thesis successfully.

I would also like to thank the members of the research group (AI4EO) at DLR, including the Team lead, fellow researchers, and colleagues, for their support, insightful feedback, and suggestions throughout the development of this thesis.

A special thanks to my husband for his understanding, encouragement and constant support during my studies and while preparing this thesis, and to my family for all the love, patience, encouragement and constant support throughout my education.

Lastly, I owe special thanks to all those who helped in any way to finish this thesis. Thank you for your support and encouragement.

List of Abbreviations

ADM – Administrative Division

CEMS – Copernicus Emergency Management Service

DLR – Deutsches Zentrum für Luft- und Raumfahrt

DN – Digital Number

ESA – European Space Agency

EI – Exposure Index

GDP – Gross Domestic Product

GIS – Geographic Information System

GNI – Gross National Income

HDI – Human Development Index

IoU – Intersection over Union

IPCC – Intergovernmental Panel on Climate Change

IW – Interferometric Wide Swath

MSI – Multi-Spectral Instrument

NASA – National Aeronautics and Space Administration

NDWI – Normalized Difference Water Index

NGO – Non-Governmental Organization

OLI – Operational Land Imager

PPP – Purchasing Power Parity

SAR – Synthetic Aperture Radar

SDG – Sustainable Development Goal

SHDI – Subnational Human Development Index

SLC – Single Look Complex

SPID – Subnational Poverty and Inequality Database

SR – Surface Reflectance

TIRS – Thermal Infrared Sensor

UNDP – United Nations Development Program

UNDRR – United Nations Office for Disaster Risk Reduction

USGS – United States Geological Survey

VI – Vulnerability Index

WPGP – WorldPop Gridded Population Dataset.

Table of Contents

Declaration of Authorship ..... **ii**
Abstract ..... **iii**
Acknowledgement ..... **iv**
List of Abbreviations ..... **v**
1 Introduction: **1**
1.1 Objective of the Study: 4
1.2 Study Area: 5
2. Dataset: **7**
2.1 Satellite data: 7
2.2 Administrative boundaries: 8
2.3 Population data: 8
2.4 Buildings data: 8
2.5 Gross Domestic Product (GDP): 9
2.6 Poverty rate: 9
2.7 Gini Coefficient: 9
2.8 Human Development Index (HDI): 9
3. Methodology: **12**
3.1 Framework: 12
3.2 Flood inundation map: 13
3.3 Hazard: 16
3.4 Exposure: 17
3.5 Vulnerability: 18
4. Results: **20**
4.1 Flood Events of 2020 and 2025: 20
4.2 Flooded Area: 20
4.3 Flood Hazard: 24
4.4 Building Exposure: 26
4.5 Population Exposure: 28
4.6 Exposure Index: 31
4.7 Vulnerability: 32
4.7.1 Gross Domestic Product (GDP): 32
4.7.2 Poverty Rate: 34
4.7.3 Gini Coefficient: 35

4.7.4 Human Development Index (HDI): 36
4.5 Vulnerability Index: 37
4.6 Flood Risk Assessment: 38
5 Discussion and Conclusion 40
5.1 Framework Contribution: 40
5.2 Thresholding Performance: 41
5.3 Comparison of Flood Hazard Between 2020 and 2025: 42
5.4 Exposure Analysis and Exposure Index (EI): 43
5.5 Vulnerability Analysis and Vulnerability Index (VI): 43
5.6 Flood Risk Index Assessment: 44
5.7 Sustainable Development Goal (SDG) Implications: 45
5.8 Limitations and Future Research: 46
Bibliography : 47

The List of Tables

Table 1. Summary of datasets used in this thesis. 10
Table 2: Validation results of Recall, F1, and intersection over union (IoU) for the pre- and post-flood events for the year 2020 23
Table 3: Validation results of Recall, F1, and intersection over union (IoU) for the pre- and post-flood events for the year 2025 24

The List of Figures

Figure 1: Components of Risk according to the IPCC Risk Framework (IPCC, 2014) 2
Figure 2: Location of the Study Area 5
Figure 3. Workflow of the research. 12
Figure 4: (a) Water segmentation using different thresholds for water DN distribution. (b) water or non-water Segmentation [2020 (up) & 2025 (down)] 14
Figure 5: Flooding map for the 2020 event; 21
Figure 6: Flooding map for the 2025 event: 22
Figure 7: Flood Hazard for the years 2020 (a) and 2025 (b). The results are divided into five levels of severity based on percentages: 'Not affected', 'Minor affected', 'Affected', 'Major affected', and 'Highly affected' 24
Figure 8: Percentage of Flood Hazard for the years 2020 (left) and 2025 (right). 25
Figure 9: Building Exposure for the years 2020 (left) and 2025 (right). 26
Figure 10: Percentage of Building Exposure for the years 2020 (a) and 2025 (b) 26
Figure 11: The final flood map is based on the SAR image for the year 2020, including an example of building exposure using the flood map and building data for Garhi Khairo municipality, and population exposure based on the flood mask and population data for Garhi Khairo municipality. 27
Figure 12: Population Exposure for the year 2020 (left) and 2025 (right) 28
Figure 13: Percentage of Population Exposure for the years 2020 (a) and 2025 (b). 29
Figure 14: The final flood map is based on the SAR image for the year 2025, including an example of building exposure using the flood map and building data for Kandhkot municipality, and population exposure based on the flood mask and population data for Sukkur municipality. 30
Figure 15: Exposure Index for the year 2020 (a) and 2025 (b). 31

Figure 16: Normalized GDP per Capita (PPP) for the year 2020 (left) and 2025 (right). 32
Figure 17: Poverty rate for the years 2020 and 2025. 34
Figure 18: Gini Coefficient for the year 2020 (left) and 2025 (right). 35
Figure 19: HDI for the year 2020 (left) and 2025 (right). 36
Figure 20: Vulnerability Index for the year 2020 (a) and 2025 (b). 37
Figure 21: Flood Risk Map for the year 2020 (a) and 2025 (b). 38

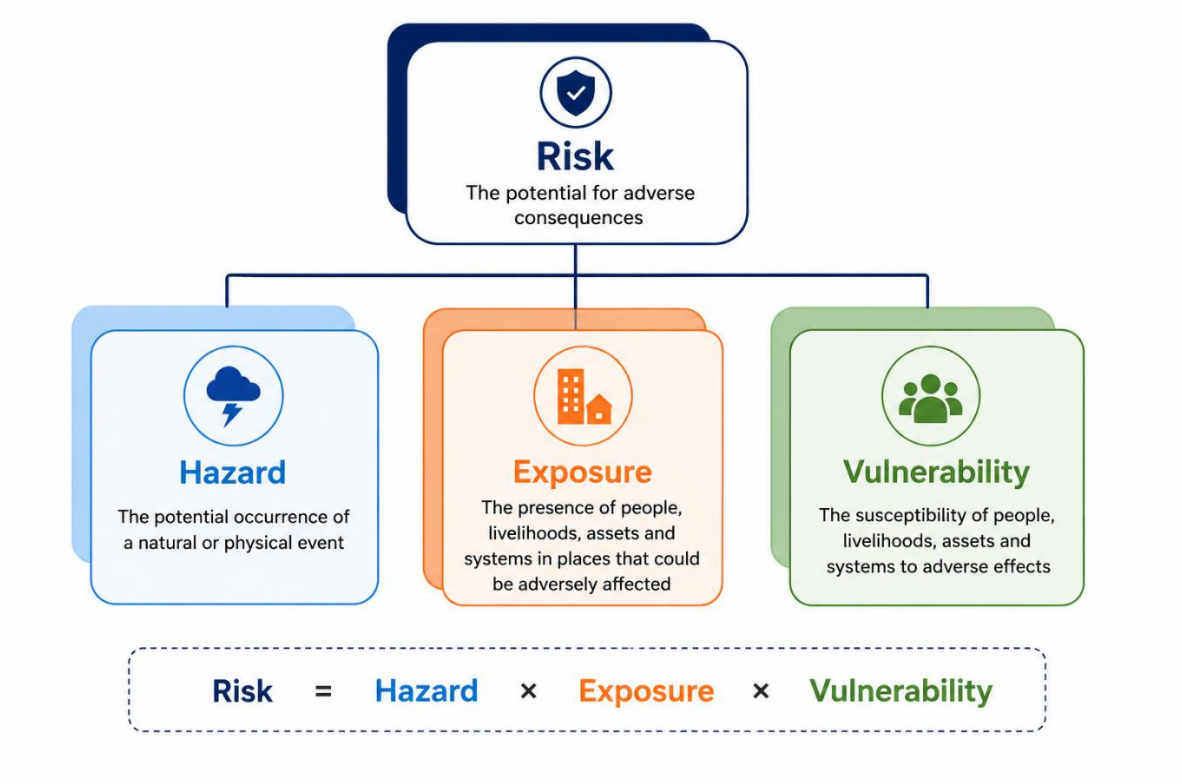
Chapter 1:

1 Introduction:

Global climate change is bringing more extreme weather events to the world, which is causing a greater social, economic, and environmental impact (IPCC, 2022). Floods are one of the most common and devastating disasters among natural hazards, impacting millions of people each year and resulting in significant damage to infrastructure, agriculture, and livelihoods (UNDRR, 2023). The rising temperatures, changes in precipitation patterns, the sea-level rise, the rapid urbanization, and population growth are expected to cause an additional rise in flood exposure and consequent economic losses over the next few decades (Winsemius et al., 2016). So, improving the assessment of flood risk is crucial for implementing effective disaster-risk reduction and climate adaptation strategies.

Due to monsoon climate, numerous rivers, and dependence on the Indus Basin, Pakistan is highly prone to flooding. Sindh Province in the lower Indus Basin is one of the most flood-prone provinces of the country because of low-lying topography, large agricultural area, and growing urbanization (Rahman & Shaw, 2015). Floods have often caused serious damage to infrastructure, agricultural production, and local communities. In developing countries such as Pakistan, the frequency of floods is increasing, population is growing fast, urban expansion, and socio-economic inequalities contribute further to exacerbate disaster risk in this country (ADB, 2021). Climate change increases hydrological extremes by the perturbation of the water cycle, a warmer atmosphere can hold more moisture; it becomes more crucial to identify which regions/municipalities are most at risk for effective emergency response, disaster preparedness, and recovery planning.

For effective flood risk management, not only do we need timely information on where floods occur, but we also need rapid information on which communities, buildings and populations are being affected by the flooding. The Intergovernmental Panel on Climate Change (IPCC) has found that the risk of disaster is the result of the interaction between hazard, exposure, and vulnerability (IPCC, 2014). Hazard actually represents the physical characteristics of a flood, exposure describes the population and assets in the flood hazard area, and Vulnerability is how much the communities are vulnerable to the impacts of flooding, and their abilities to recover from the event (Birkmann et al., 2013).



(Source: IPCC, 2014)

Figure 1: Components of Risk according to the IPCC Risk Framework (IPCC, 2014)

Satellite imagery is an effective tool for rapidly monitoring flood events, particularly near their peak intensity, due to its ability of providing rapid and consistent observations over large geographic areas. In particular, Synthetic Aperture Radar (SAR) sensors, including Sentinel-1, are very useful because they can capture images even under cloudy conditions and at night (Schumann & Di Baldassarre, 2010). Optical sensors such as Sentinel-2 and Landsat 8 provide support to SAR observations and are common tools used for detecting and validating floods using spectral water indices, such as the Normalized Difference Water Index (NDWI) (McFeeters, 1996). Several studies have demonstrated the effectiveness of satellite imagery for flood mapping and emergency-response applications (Martinis et al., 2009; Twele et al., 2016; Giustarini et al., 2015). The number of freely available satellite data has greatly enhanced the ability of scientists and policy makers to monitor floods and determine their impact.

A number of studies have developed integrated approaches to assessing flood risk based on a combination of hazard, exposure and vulnerability. Winsemius et al. (2016) estimated the global risk of flood events, combining flood hazards, population and building exposure, and found that exposure was a significant factor in future flood losses. Birkmann et al. (2013) pointed out that vulnerability can be taken into account together with hazard as social and economic factors play

a significant role in the impact of disaster. The vulnerability is as important as the hazard, as disaster impacts are greatly influenced by social and economic conditions, Birkmann et al. (2013) noted. Cutter et al. (2003) demonstrated that, even when hazards are the same, the impacts are different due to the differences in socio-economic vulnerability of the communities.

While much work has been done in flood-risk research, there are still many challenges to be addressed. There are a number of existing frameworks based on detailed local data which is not always available in developing countries, or which are largely based on regional and national levels, rather than administrative areas. In addition, the integration of freely available satellite imagery with open datasets of socio-economic data is limited to a few practical solutions. Consequently, there is a need for flexible frameworks that can help to quickly identify municipalities that need more support after flood events without requiring a lot of data.
This study fills this gap by creating an integrated framework for the evaluation of flood hazard, exposure, vulnerability and overall flood risk at municipality level. The flood hazard is derived from Sentinel-1 SAR images, while Sentinel-2 and Landsat 8 optical images are used to validate the data. Exposures are measured based on populations and building information, and vulnerabilities are calculated using socio-economic indicators such as Gross Domestic Product (GDP), poverty rate, Gini coefficient, and Human Development Index (HDI). Each of these components contributes to a Flood Risk Index, which helps to identify municipalities with the highest flood risk and thus should be given priority.

The proposed framework could help with disaster-management planning, emergency-response strategies, and resource allocations through a full evaluation of flood impacts. Moreover, it has been applied to Sustainable Development Goal (SDG) 11 (sustainable cities and communities), by helping with flood-risk planning and reducing disaster risks. The framework also helps achieve SDG 13 (Climate Action) by improving capacity-building for climate-risk assessment and adaptation planning for climate-related hazards (United Nations, 2015). The methodology uses freely available satellite imagery, open geospatial data, and reproducible analytical steps, making it suitable for other flood-prone and data-limited regions around the world.

Our research framework is the extension of the work based on the satellite imagery-driven resource allocation concept (Framework) developed by Eudaric et al. (2024). Their approach involved an Exposure Index (EI) that combined building exposure and population exposure, and flood hazard to rapidly allocate post-flood resources. This framework is extended in this research to a more comprehensive flood risk assessment framework. Apart from hazard and

exposure, a Vulnerability Index (VI) was also included, based on GDP, the Human Development Index (HDI), the poverty rate, and the Gini coefficient. Incorporating these socio-economic factors allows for the evaluation of the physical effects of flooding, as well as how well communities can prepare for and recover from flooding.

In order to map flooding areas within selected study regions, a consistent satellite-based workflow was implemented. As flood occurrences and data availability differed from region to region, two flood events were examined in Region Sindh in Pakistan. For the purpose of ensuring consistency and comparability of results, we applied the same flood mapping methodology to the region and event in our study.

1.1 Objective of the Study:

The main aim of this thesis is to develop a framework for assessing the flood risk and its impacts with the help of satellite data and socio-economic data. In this study, Northern Sindh Province in Pakistan is taken as a case study to demonstrate the application of the framework. The framework is designed to be applicable across other flood-prone areas, particularly in low and lower-middle-income countries, and will contribute to Sustainable Development Goals (SDGs) 11 and 13.

The specific objectives of the study include:

(i) mapping flood hazards using multi-sensor satellite data, and "computer vision–based" thresholding techniques (e.g., Otsu and Triangle, Standard Deviation, and Threshold Minimum methods).

(ii) determining the exposure of the population and buildings to flooding.

(iii) evaluating socio-economic vulnerability using indicators such as the GDP, Gini coefficient, poverty rate, and the Human Development Index (HDI).

(iv) creating a comprehensive Flood Risk Index to support disaster management planning, emergency response strategies, and resource allocation purposes.

This thesis is divided into five chapters, and their contents are shown as follows:

- ✓ Chapter 1: Introduction. It mainly talks about the background, problem, and objectives of the thesis as well as about the study area.

- ✓ Chapter 2: Dataset: It explains which dataset is used, for example, Satellite Imagery, Gridded data
- ✓ Chapter 3: Methodology. It deeply explains the theoretical background knowledge used in this thesis, including the threshold technique: Otsu, Triangle, Standard Deviation, and Minimum.
- ✓ Chapter 4: Results. It illustrates the experimental results found after applying the threshold technique.
- ✓ Chapter 5: Discussion and conclusions. It concludes the thesis and discusses the limitations and future directions of this topic.

1.2 Study Area:

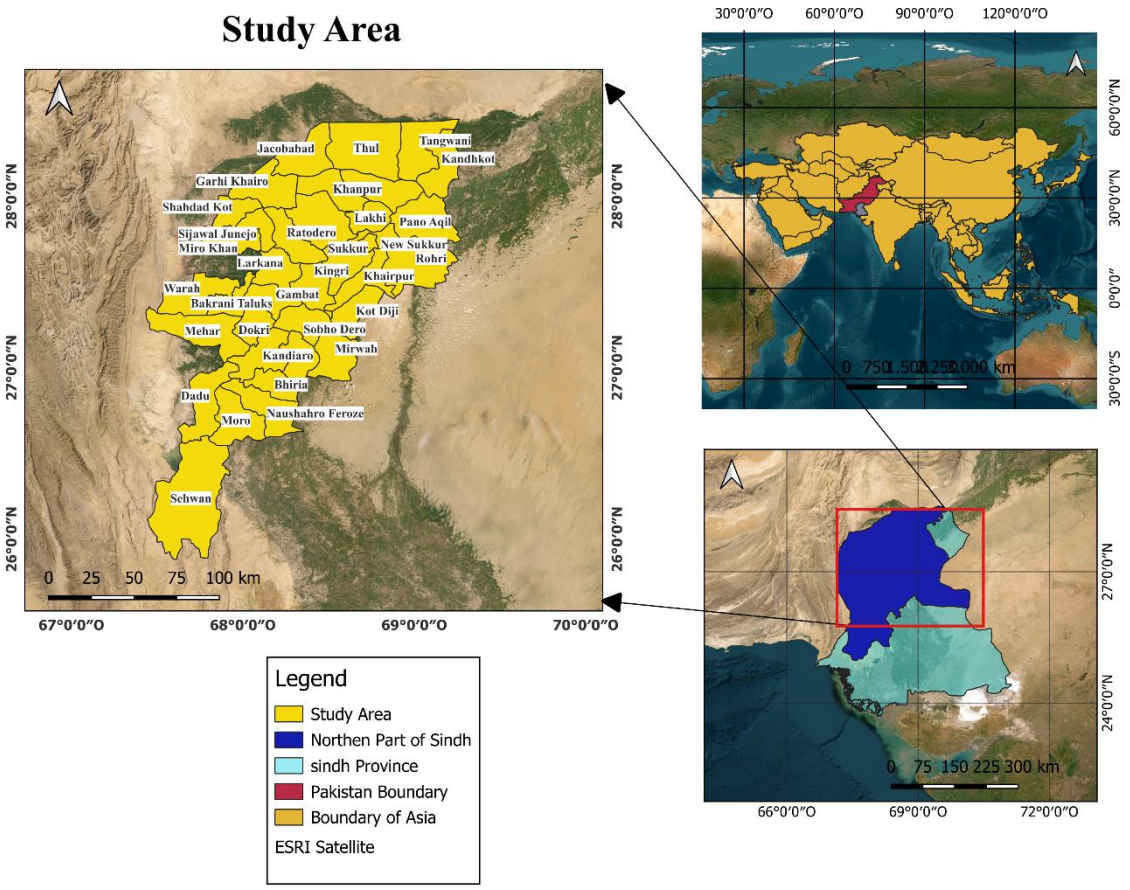


Figure 2: Location of the Study Area

The primary focus of this research is the Sindh Province in Pakistan, specifically its northern municipalities. For the purpose of spatial analysis, the study utilizes administrative boundaries at the municipality scale, obtained through DIVA-GIS.

This research is based on the northern part of Sindh Province, Pakistan, with a total of 36 municipalities covering a substantial area of the Lower Indus Basin (Figure 2). The area with a latitude ranging from 26°N to 29°N and a longitude from 67°E to 70°E. Sindh has been identified as one of the most flood-prone regions in Pakistan as it is a low-lying region, has many river systems, and depends on monsoon rains for water (NDMA, 2023). The study area covers both highly populated urban areas and mostly agricultural municipalities, which allows an examination of the differences in flood hazard, exposure, vulnerability, and risk.

In recent decades, Northern Sind has faced several significant flood events, which have led to significant damage to infrastructure, agriculture, and local livelihoods (Biswas et al., 2025). The Indus River system is important; it affects agriculture and economic development, but also puts the region at risk of river flooding during periods of extreme rainfall (Rahman & Shaw, 2015). Floods can have significant economic and social impacts on communities, particularly since agriculture is a significant economic activity in the region (Government of Pakistan, 2023).

This study focused on the municipality because the management of flood risk, response to emergencies, and resource allocation are typically carried out at the local administrative level. Therefore, the municipality-level analysis is important to find the high-risk areas and support disaster-management planning.

Chapter 2

2. Dataset:

2.1 Satellite data:

In this study, multi-mission satellite images were used for flood mapping, such as Sentinel-1 SAR, Sentinel-2, and Landsat 8 data. Sentinel-1 Synthetic Aperture Radar (SAR) data was employed as the main data source for flood mapping because Sentinel-1 SAR can acquire images in all weather conditions and at day/night, and is able to penetrate cloud cover, which is especially beneficial in flood situations (Schumann & Di Baldassarre, 2010). Additional validation and reference flood mapping were also performed using Sentinel-2 Level-2A Surface Reflectance products and Landsat 8 Collection 2 Level-2 Surface Reflectance (SR) optical imagery using the Normalized Difference Water Index (NDWI) (McFeeters, 1996).

The Sentinel missions belong to the European Space Agency's (ESA) Copernicus Program, and Landsat 8 is operated by NASA and the US Geological Survey. We chose these datasets because they are freely available and easy to access worldwide. This makes our framework more reproducible and useful for disaster management.

Sentinel-1: The satellite Sentinel-1A was launched on April 3, 2014, followed by the satellite Sentinel-1B, which was launched on April 25, 2016. Because Sentinel-1B is not operational, the revisit time is estimated at about 12 days. In our study, data, we utilized from Sentinel-1 Interferometric Wide Swath (IW), featuring dual polarization (VV, VH) and covering a 250 km swath with a spatial resolution of 5 by 20 meters in single look complex (SLC) format for flood mapping. The Sentinel-1/2 imagery data, which we used here, was obtained from the Copernicus Data Space Ecosystem website (https://dataspace.copernicus.eu/explore-data/data-collections/sentinel-data/),

Sentinel-2: The Sentinel-2 (S2) mission consists of two polar Earth orbiting optical satellites, Sentinel-2A (launched on 23rd of June 2015) and Sentinel-2B (on 7th of March 2017), which are phased by 180^0 to maximize their observing capability. The Multi-Spectral Instrument (MSI) has 13 spectral bands ranging from 43 nm to 2190 nm, four of which have a spatial resolution of 10 m, 6 bands with 20 m resolution, and 3 bands with 60 m resolution, with a swath of 290 km. The revisit frequency of a single S2 satellite is 10 days, so the combined revisit of the constellation is 5 days (eoPortal, 2018). The Sentinel-2 imagery data, which we used here, was obtained from the Copernicus Data Space Ecosystem website (https://dataspace.copernicus.eu/explore-data/data-collections/sentinel-data/).

This study employed the Level-2A product, which delivers atmospherically corrected Surface Reflectance (SR) images.

Landsat 8: Landsat 8 optical data was launched in a joint mission between NASA and the United States Geological Survey (USGS) on February 11, 2013. Landsat 8 is equipped with 11 spectral bands from the Operational Land Imager (OLI) and Thermal Infrared Sensor (TIRS). The OLI has multispectral data at 30 m spatial resolution, and the panchromatic data is at 15 m resolution. The revisit time of Landsat 8 is 16 days. Landsat 8 Collection 2 Level-2 Surface Reflectance (SR) imagery for NDWI analysis. The Level-2 product delivers atmospherically corrected surface reflectance data at 30 m spatial resolution, which are suitable for flood mapping and water-body extraction. The Landsat 8 imagery data, which we used here, was obtained from the USGS EarthExplorer platform (https://www.usgs.gov/landsat-missions/landsat-data-access).

2.2 Administrative boundaries:

The aim of this study was to evaluate the flood risk at the municipality level, so the administrative boundaries were taken from the DIVA-GIS database (Diva_gis, 2000). The hazard, exposure, vulnerability, and flood-risk indicators have been calculated and compared across municipalities using these boundaries.

2.3 Population data:

We used the WorldPop High-Resolution Population dataset (WPGP) developed by the University of Southampton (Tatem, 2017) to estimate the population density. This dataset contains geographical information about the population and is available in detail and in an accessible format. The Population datasets have been taken from this website (https://www.worldpop.org/). The data consists of spatial information (people count per grid cell), with a spatial resolution of 3 arc-seconds. This dataset covers the globe, and the time range is from the year 2000 to 2020. Population estimations are provided at a resolution of about 100 m and 1 km for the year 2020, and estimates of the number of people in each age-sex group. The population data used for exposure analysis in this study were at a 100 m resolution.

2.4 Buildings data:

In our analysis, the Building Footprints dataset from Microsoft (Microsoft, 2022) was used to evaluate the building numbers, spatial distribution, and to assess building exposure within the study area. The Building Footprints dataset from Microsoft has been downloaded from this website (https://github.com/microsoft/GlobalMLBuildingFootprints). In this dataset, you can find digital maps of building shapes that are created from clear Maxar satellite images and then

analyzed using advanced computer methods (deep learning) to find out their outlines. A total of over 1.3 billion building footprints were globally identified from 2014 to 2023.

2.5 Gross Domestic Product (GDP):

GDP data (Downscaled gridded global dataset for gross domestic product (GDP) per capita PPP) : We used the Downscaled Gridded Global GDP per capita (PPP) dataset to obtain GDP per capita data (Kummu et al., 2025). Data are available at the ADM2 level and 5 arc-minute spatial level for the period 1990-2022. Detailed datasets are available in the Scientific Data repository (Kummu et al., 2025). http://www.nature.com/articles/s41597-025-04487-x#Sec12.

2.6 Poverty rate:

The poverty data utilized in this study was provided by the World Bank's Subnational Poverty and Inequality Database (SPID) (World Bank, 2024). This database provides estimates of poverty and inequality at the sub-national level in regions of countries across the world, providing socio-economic analysis at the regional and local levels. The international poverty line of $3.00 per day (2021 PPP) was used as an indicator of socio-economic vulnerability for our research. The data is available on the World Bank Poverty and Inequality Platform (PIP) Interactive Maps: https://pipmaps.worldbank.org/en/data/datatopics/poverty-portal/poverty-interactivemap.

2.7 Gini Coefficient:

Gini data (Global subnational Gini coefficient (income inequality) per capita PPP datasets), we used the Global Subnational Gini Coefficient dataset to measure income inequality Kummu et al. (2025). This dataset provides estimates of the Gini coefficient at the subnational (ADM1) level for each year between 1990 and 2023. It offers a consistent view of income inequality across regions and over time. The Gini coefficient values for 2020 were used for the 2020 flood analysis, and the most recent data available (2023) has been applied to the 2025 analysis. The data used in the study was retrieved from the study by Chrisendo et al. (2025) and accessed from the corresponding Zenodo repository: (https://zenodo.org/records/16410778)

2.8 Human Development Index (HDI):

The data on the Human Development Index (HDI) were sourced from the database of Global Data Lab Subnational Human Development Index (SHDI) (Smits & Permanyer, 2019). The dataset offers estimates of the HDI on an annual basis at the subnational level, based on indices of health, education, and living standards. The HDI values for 2020 were used for the 2020 flood analysis, whereas the most recent data available (2023) has been applied to the 2025

analysis. HDI dataset is available at this link: https://www.nature.com/articles/s41893-025-01689-4#Sec19

Table 1. Summary of datasets used in this thesis.

Dataset / Sensor	Data Type	Spatial Resolution	Revisit Time	Acquisition Date (Pre-Flood)	Acquisition Date (Post-Flood)	Purpose	Source
Sentinel-1 (2020)	SAR (VV, VH) IW	5 m × 20 m	12 days	06 April 2020	28 August 2020	flood mapping and change detection	Copernicus Data Space Ecosystem
Landsat 8 (2020)	Optical	30 m	16 days	08 April 2020	31 August 2020	NDWI validation and reference mapping	USGS / NASA
Sentinel-1 (2025)	SAR (VV, VH) IW	5 m × 20 m	12 days	04 April 2025	19 September 2025	flood mapping and change detection	Copernicus Data Space Ecosystem
Sentinel-2 (2025)	Optical MSI Level-2A	10 m, 20 m, 60 m	5 days	07 April 2025	19 September 2025	NDWI validation and reference mapping	Copernicus Data Space Ecosystem
WorldPop Population Data	Gridded population	100 m	Annual	2020	2020	Population exposure analysis	University of Southampton
Microsoft Building Footprints	Building outlines	Variable	Updated periodically	2014–2023	2014–2023	Building exposure analysis	Microsoft & Maxar
GDP Dataset	Socio-economic	Gridded	Annual	2020–2025	2020–2025	Economic vulnerability assessment	World Bank

Dataset / Sensor	Data Type	Spatial Resolution	Revisit Time	Acquisition Date (Pre-Flood)	Acquisition Date (Post-Flood)	Purpose	Source
Poverty Rate (SPID)	Socio-economic	Administrative level 1	Periodic	2018 baseline	2018 baseline	Poverty vulnerability analysis	World Bank SPID
Gini Coefficient Dataset	Socio-economic	Administrative level 1	Periodic	Latest available	Latest available	Income inequality assessment	Global Data Lab
HDI Dataset (SHDI)	Socio-economic	Administrative level 1	Annual	Latest available	Latest available	Adaptive capacity assessment	Global Data Lab

Chapter 3:

3. Methodology:

3.1 Framework:

This research utilized a quantitative risk assessment framework to analyze the effects of flood event. We want to apply this framework rapidly in the aftermath of the flood event using satellite images. This main method uses a standard risk equation to figure out the final Flood Risk Index, which is made up of three different factors: Hazard, Exposure, and Vulnerability (IPCC, 2014).

Risk = Hazard x Exposure x Vulnerability…….(1)

This project aims to develop a rapid and accurate assessment framework that can be used everywhere, especially in low- and low-middle-income countries.

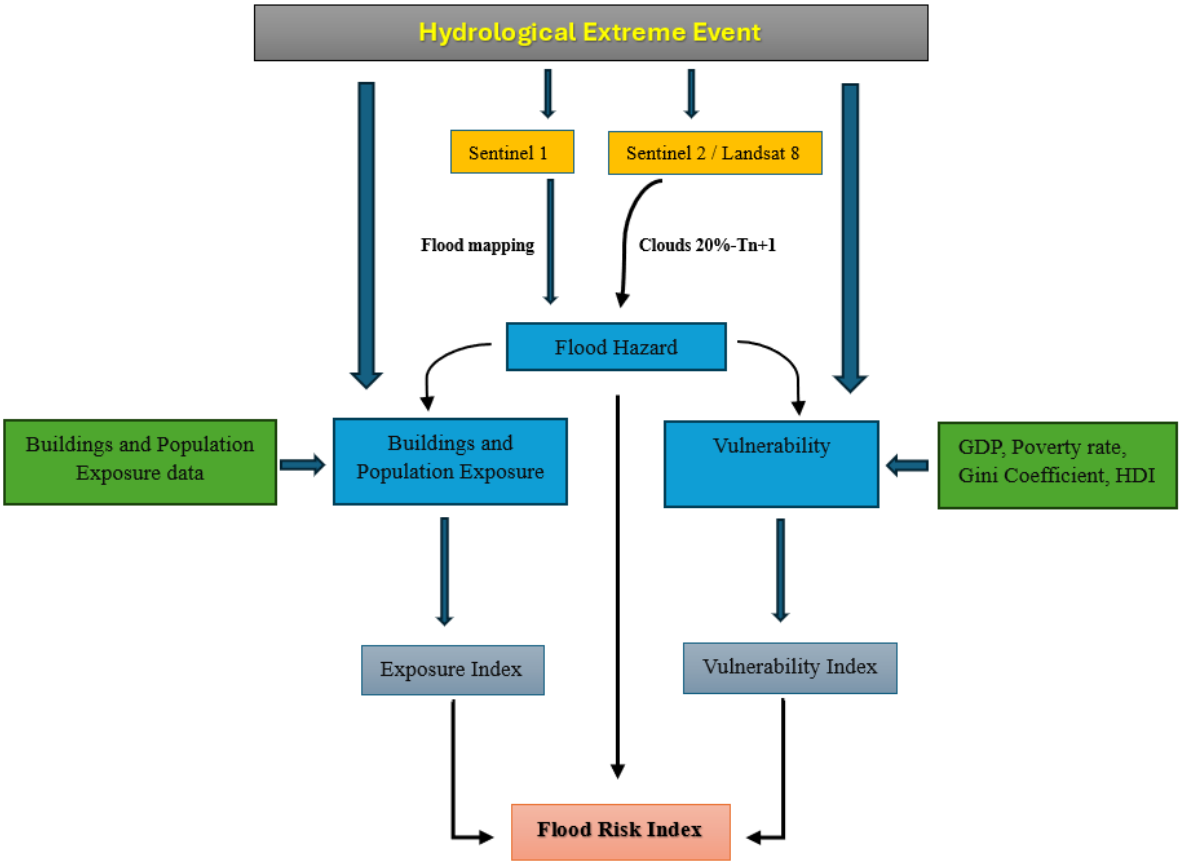


Figure 3. Workflow of the research.

The overall workflow of the flood risk assessment framework adopted in the study is shown in Figure 3. After a hydrological extreme event, the flood extent is mapped using Sentinel-1

imagery, and the Flood Hazard is generated from this data. Then validated using the Sentinel-2 imagery and Landsat 8 imagery when available. The Exposure Index (EI) is developed by combining population and building datasets to estimate the exposure. The Vulnerability Index (VI) is calculated from a combination of socio-economic indicators such as GDP, Human Development Index (HDI), poverty rate, and Gini coefficient. Finally, Hazard, Exposure, and Vulnerability are combined to calculate the Flood Risk Index for rapid post-flood risk assessment, resource allocation, and planning for disaster management.

3.2 Flood inundation map:

To ensure the availability of flood data regardless of weather conditions, we used Synthetic Aperture Radar (SAR) data. In order to analyze the Flood inundation map, we utilized the Sentinel-1 Synthetic Aperture Radar (SAR) preprocessed images, which were obtained from the Copernicus Data Space Ecosystem (https://dataspace.copernicus.eu/explore-data/data-collections/sentinel-data/). SAR penetrates the cloud as microwaves, so we could capture the flood inundation map close to the pic of the flood, where we can observe high cloud accumulation. Prior to downloading, the SAR images are first processed by the ecosystem to prepare them, which involves orbit file adjustments, radiometric calibration, the removal of thermal noise, de-bursting, multi-looking, speckle filtering, and terrain correction (NASA Earthdata, 2019 & Eudaric et al., 2024).

The pixel intensity values of Sentinel-1 SAR images were used to identify flooded areas. The Digital Number (DN) of each pixel in the SAR data corresponds to the strength of the radar backscatter received from the Earth's surface (Tran et al., 2022; Martinis et al., 2009). In general, the DN values at open water surfaces are low because of specular reflection, whereas the DN values of rough surfaces like vegetation and urban areas are high because of a stronger backscatter response.

The digital number DN shows the intensity of electromagnetic energy measured for the ground resolution cell, which each pixel in the image represents (Ulaby et al., 2014). Basically, the higher DN in a SAR image pixel indicates strong backscatter, whereas a lower DN shows weak backscatter. Surface water has specific reflectance characteristics that lead to lower backscatter values (Eudaric et al., 2024). This allows for quick differentiation between the foreground and background in an image and creates a binary mask of water and non-water. Researchers often use thresholds on SAR images to map flood hazards (Martinis et al., 2009; Twele et al., 2016). Different processing methods can lead to variations in the frequency distribution of grey-level

values, which are represented as a histogram (Sezgin & Sankur, 2004). The effectiveness of thresholding in SAR image analysis depends on the unique features and properties of the image being analyzed. Thus, testing multiple thresholds is essential for getting reliable results (Eudaric et al., 2024). In our study, we use four different thresholding methods to compare images before and after the event: Standard Deviation (Li & Liu, 2009), Triangle (Zack et al., 1977), Threshold Minimum (Prewitt & Mendelsohn, 1966), and Otsu (Otsu, 1979). Pixels below the threshold are classified as water, while those above are classified as non-water. We applied a pixel-based change detection method to create the flooded mask. This process involved subtracting the pre-disaster images from the post-disaster images and choosing the threshold that provided the best results for each image (Singh, 1989; Lu et al., 2004).

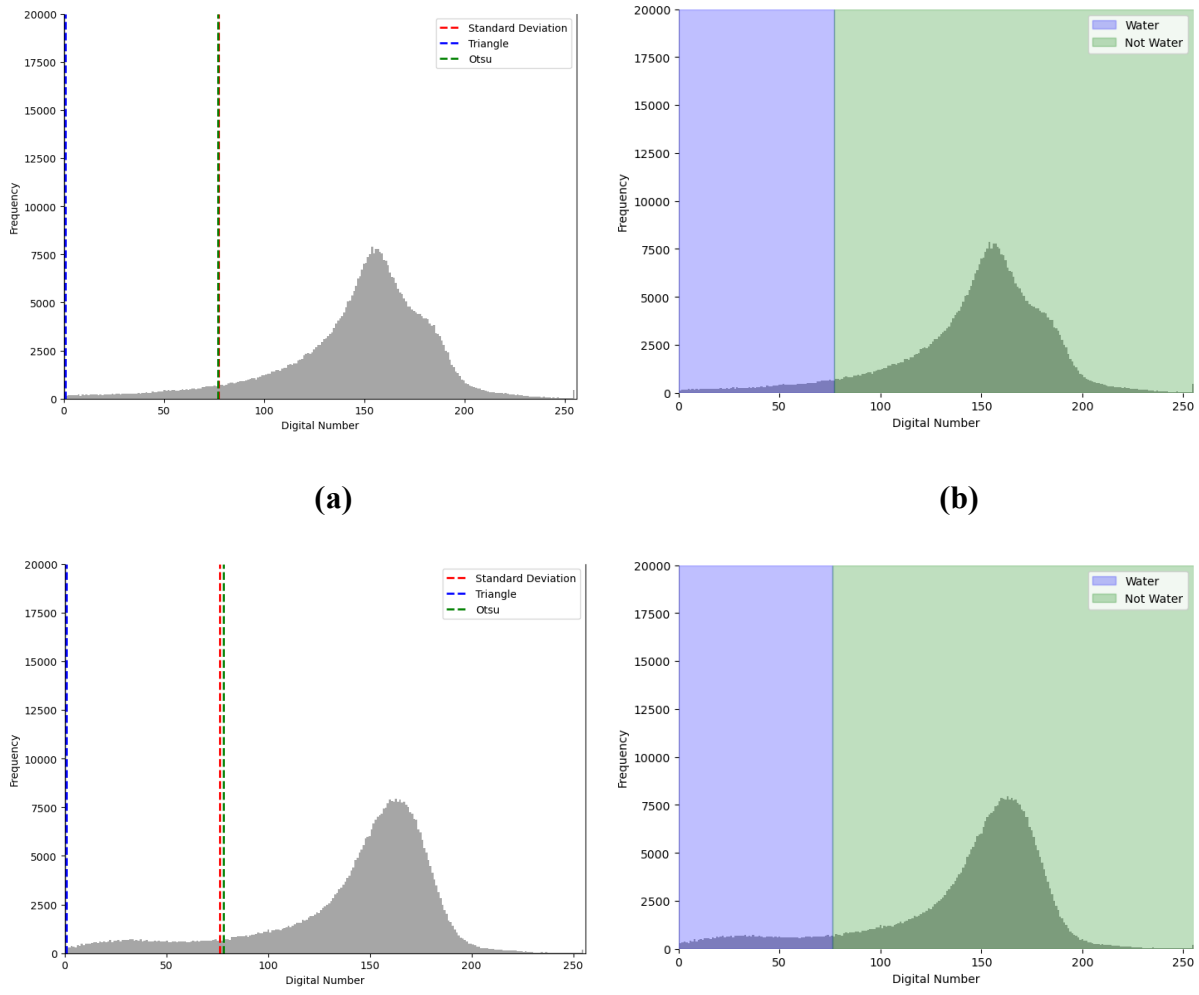


Figure 4: (a) Water segmentation using different thresholds for water DN distribution. (b) water or non-water Segmentation [2020 (up) & 2025 (down)]

It's challenging to check the accuracy of flood maps created with synthetic aperture radar (SAR) since there is often no reliable ground truth data. This is especially true during floods when it's

impossible to get field data (Notti et al., 2018; Amitrano et al., 2024). Validation is further harder because different types of land cover behave differently and there aren't always consistent observations across time. It is tricky to compare SAR flood extent products when there isn't any common reference data (Landwehr et al., 2024). Because backscatter works in a complicated way, SAR also has problems finding water in cities and places with plants. To fix these flaws, validation often needs more optical data or more information (Schumann et al., 2018; Mason et al., 2012).

Another source of validation is optical satellite data; however, cloud cover, atmospheric disturbances, and changing lighting conditions sometimes limit its usefulness during flood events (Li et al., 2019). Because of this, only a few optical images that were taken during or soon after the flood event might be suitable for study. In this study, the validation of the SAR-derived flood maps was performed with cloud-free (≤ 20%) optical satellite images from Sentinel-2 and Landsat 8. On the basis of optical data, the Normalized Difference Water Index (NDWI) was calculated in order to determine the presence of surface water. NDWI (Normalized Difference Water Index) is a spectral index often used in remote sensing for identifying and monitoring open water bodies. This is calculated using reflectance values from Sentinel-2 imagery in the green and near-infrared bands by following equation (McFeeters, 1996):

$$\mathbf{NDWI = \{(Green - NIR)\} / \{(Green + NIR)\}\ldots\ldots\ldots(2)}$$

As part of the evaluation process, we use several metrics in order to analyze the flood map that is created using our method, including intersection over union (IoU), recall, and F1. Using these metrics allows us to identify potential errors and determine the sensitivity of binary segmentation by identifying potential errors.

The IoU here indicates how well the predicted flood map matches with the ground truth, reflecting their spatial agreement. Recall, which focuses on the count of true positive detections, helps us evaluate how effectively the method identifies flood-prone areas. To assess performance levels, the F1 score, which integrates both precision and recall, offers a comprehensive measure of effectiveness (Eudaric et al., 2024). In order to improve the accuracy of flood maps, a reliable framework has been developed for combining these metrics in order to create more accurate flood maps.

$$IoU = \frac{TP}{TP + FP + TN} \quad \text{.....(3)}$$

$$Recall = \frac{TP}{TP + FN} \quad \text{.....(4)}$$

$$Precision = \frac{TP}{TP + FP}$$

$$F1 = 2 \times \frac{Precision \times Recall}{Precision + Recall} \quad \text{.....(5)}$$

Where,

In the context of pixels classification,

True Positive (TP) refers to pixels that are correctly classified as water,

False Positive (FP) refers to pixels that are correctly classified as non-water,

True Negative (TN) refers to pixels that are correctly classified as non-water, and False Negative (FN) refers to pixels that are incorrectly classified as water.

3.3 Hazard:

Flood hazard is generally defined as the possibility of injury, loss, or damage from an occurrence at a particular area **(**Kron, 2005; Seneviratne et al., 2012**).** The flood Hazard (H_i) is

expressed in Equation 6, as the proportion of the area flooded during the flood event. It shall be calculated by dividing the inundated area by the total administrative area of the spatial unit analyzed. A larger flooded proportion shows a higher flood hazard, as flooding affects more land.

Flood hazard is simply calculated by the following equation;

$$H_i = \frac{A_f}{A_t} \qquad \text{.....(6)}$$

Where:

A_f : refers to the detected water (flooded) surface area (ha).

A_t : refers to the total administrative area of the study unit (ha).

3.4 Exposure:

The term **"exposure"** refers to the condition of populations or infrastructure located within hazard-prone areas (Kreibich et al., 2022; Srivastava et al., 2023; Eudaric et al., 2024). **The Buildings Exposure** can be calculated as follows:

$$B_i = \frac{B_a\ (A_f)}{B_b} \qquad \text{.....(7)}$$

Where;

$\mathbf{B_a}$: refers to the numbers of the buildings (within the flooded region (A_f)),

$\mathbf{B_b}$: refers to the total number of the buildings

As shown in Equation 7, the buildings exposure (Bi), as evaluates the physical effects on infrastructure by this equation, is calculated based on the number of buildings that are affected by the flood hazard, and the total number of buildings in the affected area.

The term **"population exposure"** describes as the proportion of individuals impacted by floods within a specific region relative to the overall population of that region. The Population Exposure (P_i) can be calculated as follows:

$$P_i = \frac{P_a\ (A_f)}{P_b} \qquad \text{.....(8)}$$

Where:

P_a refers to the population affected; P_b refers to the total population

3.5 Vulnerability:

The concept of "vulnerability" describes how vulnerable people and systems can be negatively impacted by flood events due to underlying social, economic, and demographic factors (Birkmann et al., 2013). In contrast to hazard and exposure, vulnerability does not focus on the physical aspects of flooding on the number of impacted elements. Instead, it pertains to the sensitivity of the affected population and their ability to adapt to the circumstances.

In this research, vulnerability was evaluated by spatial socio-economic factors associated with Gross Domestic Product (GDP), poverty rate, Gini coefficient, and Human Development Index (HDI). These indicators we got from well-known worldwide datasets, like the World Bank's poverty and vulnerability mapping tools and global vulnerability databases made for climate-risk evaluation (Birkmann et al., 2013; Adger, 2006).

The Vulnerability Index is simply calculated by the following equation;

Vulnerability Index = $GDP_{_NI}$ + Poverty $rate_{_NI}$ + Gini $coefficient_{_NI}$ + $HDI_{_NI}$.....(9)

Where,

GDP refers to Gross Domestic Product,

HDI refers to the Human Development Index,

NI means that the value has been processed as Normalized Index (on a scale of 0-100)

It is significant to point out that, based on our analysis of flood hazard (Hi), building exposure (Bi), population exposure (Pi), and Gross Domestic Product (GDP), poverty rate, Gini

coefficient, and Human Development Index (HDI) results, it has been divided into five distinct severity percentage intervals, each of which is associated with a specific severity category. As a result of the class intervals, the percentages and class numbers are assigned as follows:

0 (0): "Not affected" means there is no flooding, exposure, or social and economic risk in the area;

≤25% (1): "Minor Affected" refers to minimal impact or low susceptibility, affecting only a small portion of the region, assets, or population.

≤50%, (2): "Affected" means moderate conditions where about half of the area is affected by flooding, exposure, or social and economic risk;

≤75%, (3): "Major Affected" means severe conditions where a large part of the land, people, or buildings are affected or show high risk;

≤100%, (4): "Highly Affected" means critical situations with almost complete flooding or exposure and high social and economic risk.

The analysis was carried out in QGIS, ArcGIS Pro, and Python through the Jupyter Notebook. The processing of spatial data, visualization, and map production were performed using QGIS and ArcGIS Pro, while Python was employed for thresholding, index calculations, and other statistical analysis.

Chapter 4

4. Results:

4.1 Flood Events of 2020 and 2025:

In this study, the flood extent in the northern part of Sindh Province was mapped for two major flood events in 2020 and 2025 during the monsoon period. As per reports from various national and international organizations such as NDMA, FAO, UNOCHA, and WHO, both events caused heavy floods and socio-economic consequences in Sindh Province in 2020 and 2025, respectively (NDMA, 2020; FAO, 2020; UNOCHA, 2025; WHO, 2025). For the 2020 flood event, there was severe monsoon rainfall in late August 2020, while for the 2025 flood event, there was intense monsoon rainfall and river flooding in August–September 2025. Post-flood satellite images were chosen to represent the inundated extent near the peak of the flood, to ensure the maximum possible inundation area within the study area.

The images of the flood of 2025 were acquired from Sentinel-1 satellite imagery before the flood on 4th April 2025 and after the flood on 19th September 2025 with an ascending orbit. Additionally, Sentinel-2 images were acquired before the flood on 7th April 2025 and after the flood on 19th September 2025 (Fig. 6). In the 2020 event, the images from Sentinel-1 were acquired on 6 April 2020 (before the flood) and on 28 August 2020 (after the flood), both in ascending orbit. Images acquired from Landsat 8 were used before the flood (April 8, 2020) and after the flood (August 31, 2020) (Fig. 5).

4.2 Flooded Area:

In order to map flooding areas within selected study regions, a consistent satellite-based workflow was implemented. As flood occurrences and data availability differed from region to region, two flood events were examined in the Northern Region of Sindh Province in Pakistan. For the purpose of ensuring consistency and comparability of results, we applied the same flood mapping methodology for each region and event in our study.

Our approach was to select the single post-disaster satellite image that contained the most water pixels to capture the flood at its absolute peak. We primarily used Sentinel-1 radar (SAR) imagery to map flooding before and after an event in ascending and/or descending orbits. Our

results were also validated with Sentinel-2 and/or Landsat 8 imagery by calculating the Normalized Difference Water Index (NDWI) whenever clear optical data was available.

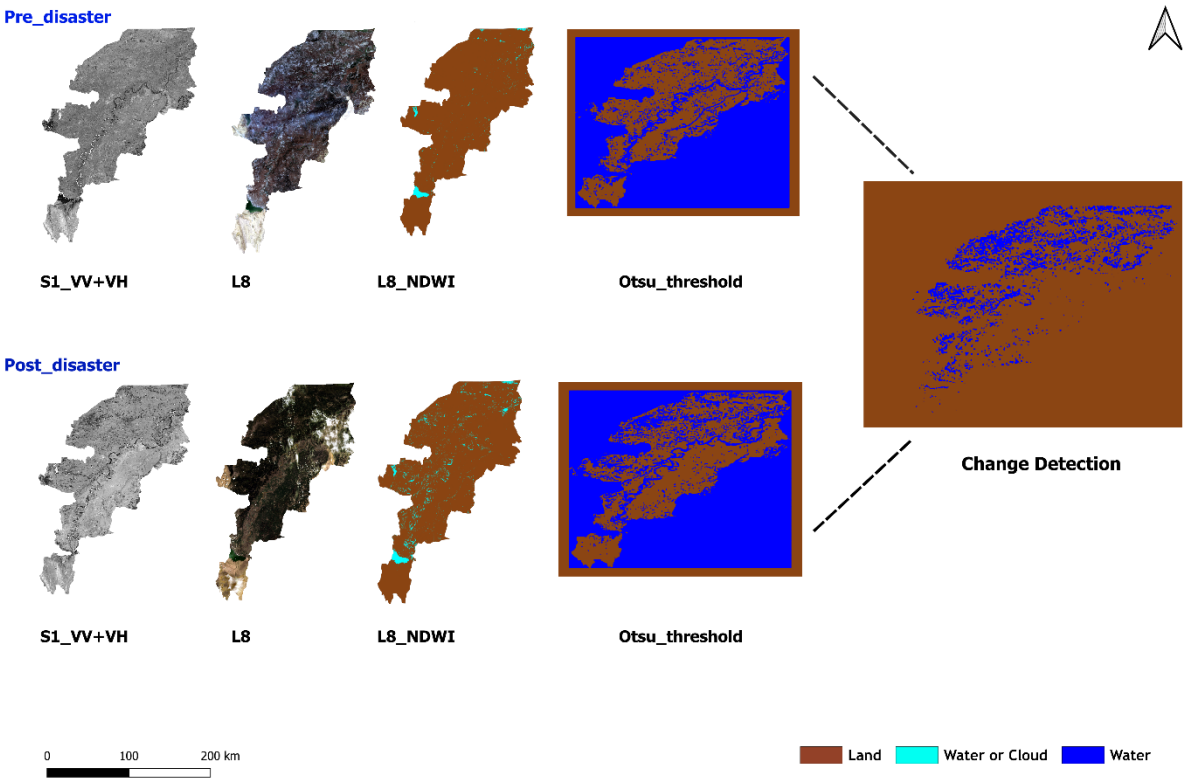


Figure 5: Flooding map for the 2020 event; The first row shows **pre-disaster images**: S1_VV+VH refers to the Sentinel-1 image, L8 is the Landsat 8 image, L8_NDWI is the Landsat 8 image processed with NDWI, and Otsu_threshold means the Sentinel-1 data is classified using the Otsu threshold. The second row shows **post-disaster images** with the same categories. Change Detection compares the pre- and post-flood images to highlight differences.

Due to the large and diverse nature of the flooded area, we encountered a major challenge. The radar does not see open fields or cities the same way as it sees cities and forests, therefore, applying one threshold to the entire map might not yield the best results. To address this, we tested four thresholding methods: Otsu, Triangle, Standard Deviation, and Minimum in order to find out which one was the most accurate at separating water from land.

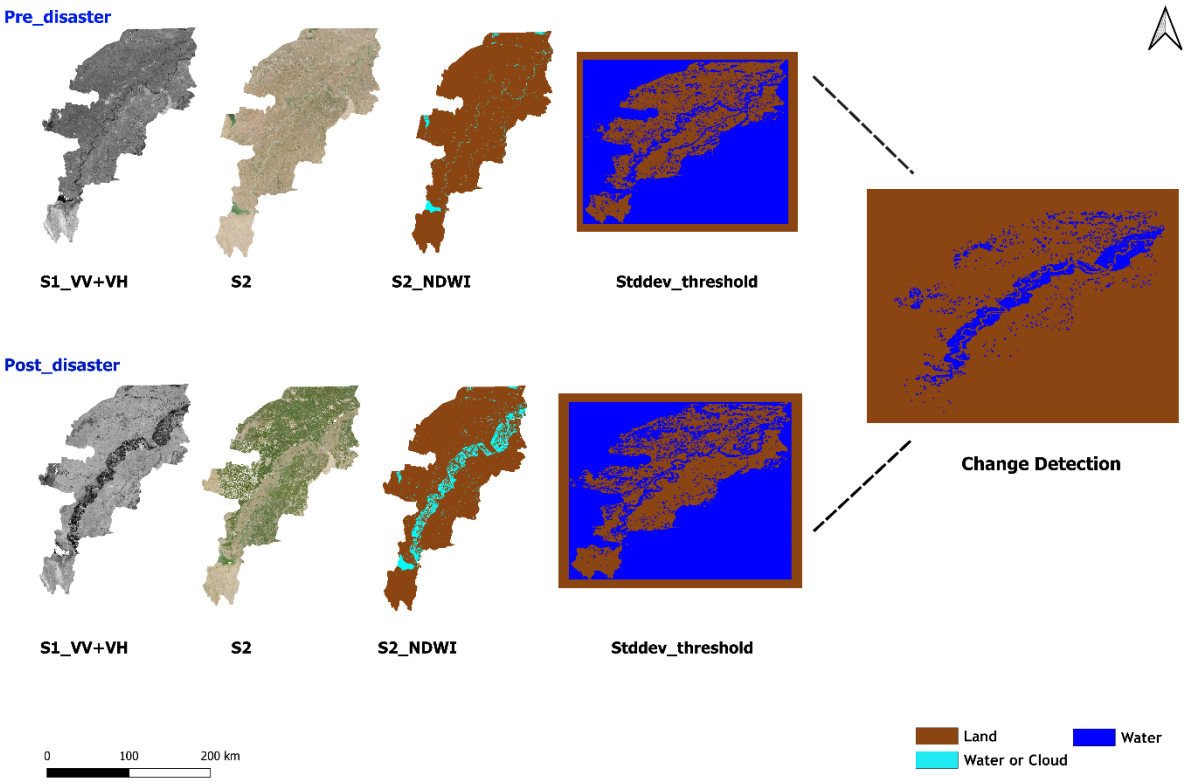


Figure 6: Flooding map for the 2025 event: The first row **(Pre-disaster)** includes S1_VV+VH (Sentinel-1 image), L8 (Landsat 8 image), L8_NDWI (Landsat 8 image based on NDWI), and Otsu_threshold (Sentinel-1 data classified using the Otsu threshold). The second row **(Post-disaster)** presents the same data types. Change Detection displays the results derived from comparing pre- and post-flood images.

By applying the four-threshold technique directly to the pre- and post-disaster SAR images, the flooded map was created. It is important to note that, in order to validate our results, we used the Normalized Difference Water Index (NDWI), which is derived from Sentinel-2's green band (B3) and near-infrared band (B8), and from Landsat 8's green band (B3) and near-infrared band (B5). For this study, we selected images with a low cloud cover (20%) in order to achieve the best possible visibility. However, it was still difficult to distinguish between clouds and water while applying the NDWI technique to these images. On satellite images, clouds often appear bright due to their similar spectral properties, which can lead to confusion when clouds exhibit high reflectance like water bodies.

The results across all regions and flood events clearly indicate that the standard deviation method is the most effective technique for creating water pixel masks. In Table 1, we are able to see the overall findings of the study. In this presence analysis, the standard deviation is an

appropriate threshold because the Digital Number (DN) appears to have a normal distribution. According to the Gaussian distribution, most of the grey level values for the water pixels are clustered around a central value, and there are very few values that deviate significantly from the mean value. Based on the results in Tables 2 and 3, it is possible to evaluate the distribution of the data and differentiate between water and non-water areas when considering the standard deviation. Even though, for some post-disaster events, the Otsu thresholding method produced better results, this is probably because the DN distribution did not follow a clear Gaussian pattern; DN histograms in these areas are irregular, making other thresholding methods more effective for separating water from non-water surfaces. After reviewing the observations, we chose the most reliable flood masks from the tested thresholding methods for each event. We applied a change-detection process by subtracting the pre-disaster water mask from the post-disaster flood masks, as described in the Methodology. This approach produced a final flooded mask for each event, serving as the foundation for hazard, exposure, vulnerability, and risk assessments across all study regions.

Table 2: Validation results of Recall, F1, and intersection over union (IoU) for the pre- and post-flood events for the year 2020:

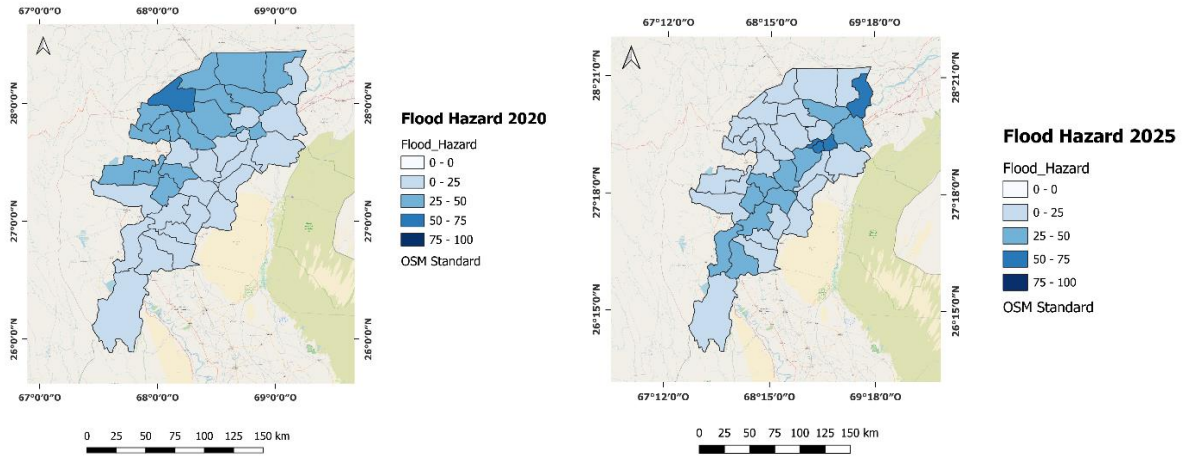
2020	**Iou pre-event**	**Iou post-event**	**Recall pre-event**	**Recall post-event**	**F1 pre-event**	**F1 post-event**
Otsu	0.75	0.71	0.75	0.85	0.73	0.70
Triangle	0.50	0.74	0.65	0.97	0.54	0.70
Standard Deviation	0.75	0.71	0.75	0.85	0.74	0.70
Threshold Minimum	--	--	--	--	--	--

Table 3: Validation results of Recall, F1, and intersection over union (IoU) for the pre- and post-flood events for the year 2025:

2025	Iou pre-event	Iou post-event	Recall pre-event	Recall post-event	F1 pre-event	F1 post-event
Otsu	0.50	0.71	0.66	0.85	0.53	0.70
Triangle	0.51	0.74	0.66	0.97	0.54	0.70
Standard Deviation	0.73	0.71	0.73	0.85	0.72	0.70
Threshold Minimum	--	--	--	--	--	--

4.3 Flood Hazard:

In our study, we assessed flood hazard for each municipality across the study regions and their respective flood events to understand the extent and severity of flooding in each area. For this purpose, we used administrative boundary data for the analysis, which were gathered from DIVA-GIS. By overlaying the flooded pixels map with municipal boundaries, we calculated the flooded area in each municipality. Based on these findings, we were then able to calculate the percentage of flood hazard for each region and event, as you can see in Figure 7.



(a) **(b)**

Figure 7: Flood Hazard for the years 2020 (a) and 2025 (b). The results are divided into five levels of severity based on percentages: 'Not affected', 'Minor affected', 'Affected', 'Major affected', and 'Highly affected'.

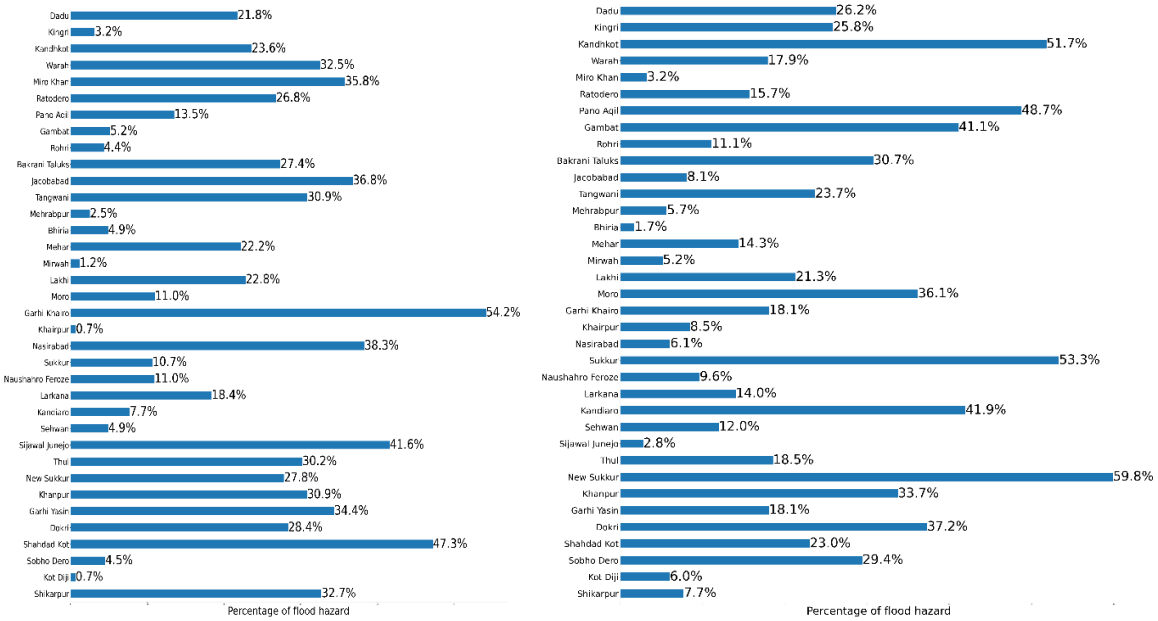


Figure 8: Percentage of Flood Hazard for the years 2020 (left) and 2025 (right).

Spatial analysis of the flood hazard maps (Fig. 7 and Fig. 8) indicates a distinct geographic shift in risk distribution across the administrative areas. Before diving into the details of each municipality, regional trends demonstrate a significant rise in overall risk. The average flood hazard across the study area increased from 20.4% in 2020 to 25.2% in 2025. This means the flood is spreading throughout the area, bringing the region closer to being classified as 'Affected'. Analysis of individual administrative units indicates that the municipalities of Garhi Khairo and Shahdad Kot were the most affected by the 2020 flood hazard, with 54.2% and 47.3% of their areas, respectively, experiencing flooding (Fig. 7, a). The flood hazard for Garhi Khairo was categorized as "Major affected" (Fig. 7, a), identifying it as the primary hotspot during that period. In contrast, municipalities such as Khairpur and Kot Diji experienced only minor impacts and were categorized as "Minor affected," with less than 1% of their area touched by floodwaters (Fig. 8).

By 2025, risk levels increased sharply in the eastern and northern areas. New Sukkur was the hardest hit, with its hazard area rising to 59.8% (Fig. 7, b), followed by Sukkur at 53.3% and Kandhkot at 51.7%. These numbers show a clear rise in risk, moving these areas into the "Major affected" (Fig. 7) category. On the other hand, Sijawal Junejo, which had a high hazard of 41.6% in 2020, dropped significantly to 2.8% by 2025 (Fig. 8), putting it in the "Minor affected" category. The findings indicate that New Sukkur, Sukkur, and Kandhkot are the municipalities facing the highest hazard levels. This change exposes key urban centers, infrastructure, and

densely populated areas to greater risk, necessitating a comprehensive reassessment of regional disaster mitigation strategies and resource distribution.

4.4 Building Exposure:

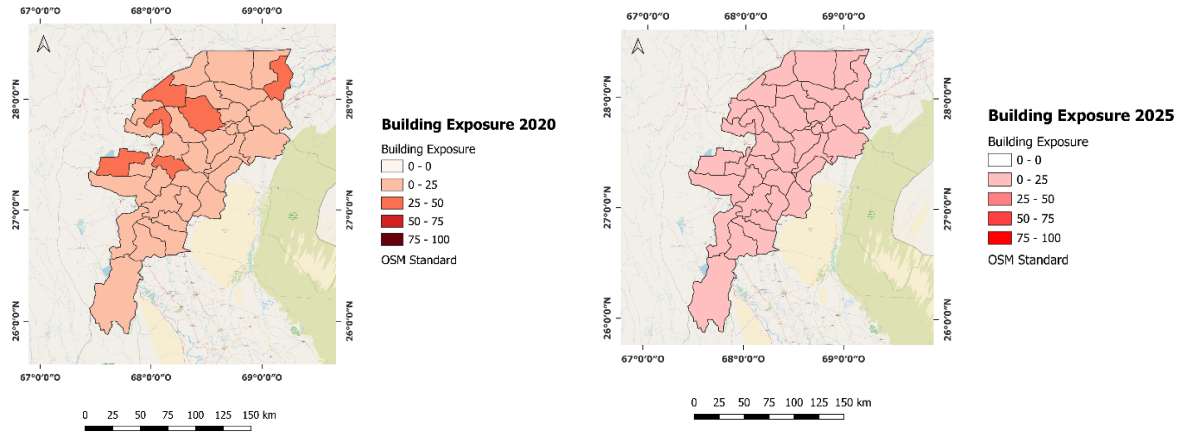
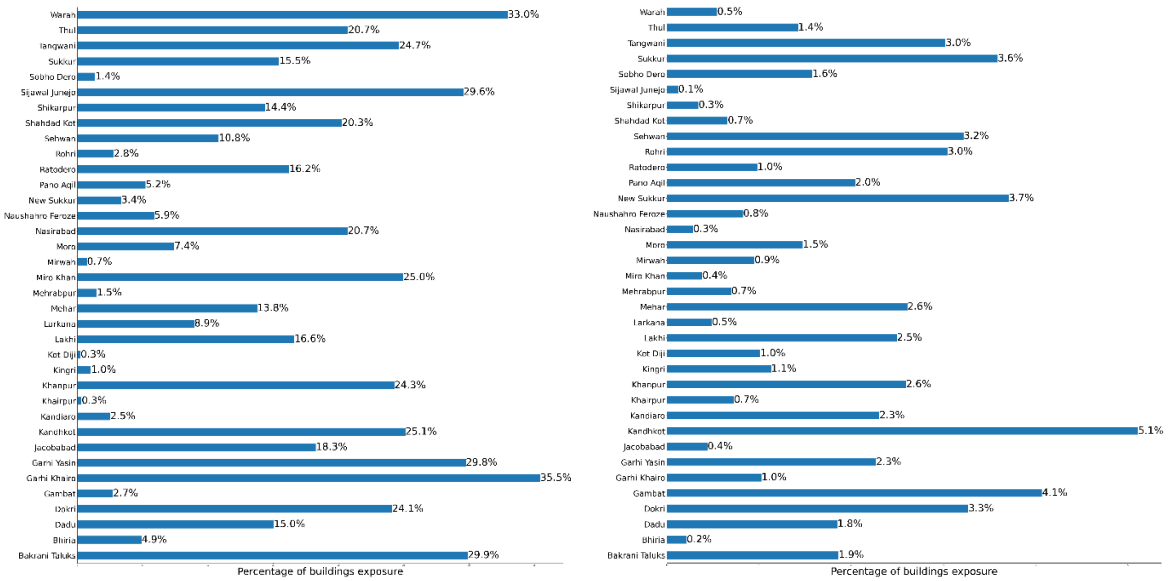


Figure 9: Building Exposure for the years 2020 (left) and 2025 (right).

Building exposure was estimated using the Microsoft Building Footprints dataset, which provides a comprehensive global collection of building outlines.



(a) (b)

Figure 10: Percentage of Building Exposure for the years 2020 (a) and 2025 (b).

Flooded buildings were identified by overlaying the pixel-based flood map with the building footprints (Fig. 11). During the peak flow of the flood in 2020, the municipality of Garhi Khairo

was the most affected, with 35.5% of buildings exposed, followed by Warah at 33.0% (Fig. 10 (a)). The findings show that Garhi Khairo was classified as "Affected" in terms of building exposure. In addition, several other areas also showed a little bit high exposure levels, including Bakrani Taluka at 29.9%, Garhi Yasin at 29.8%, and Sijawal Junejo at 29.6% (Fig. 10, a), all categorized as "Affected". Miro Khan was considered "Minor affected" with 25.0% exposure. On the other hand, in 2020, the least impacted municipalities were Kot Diji and Khairpur, both of which had very little building exposure—just 0.3%.

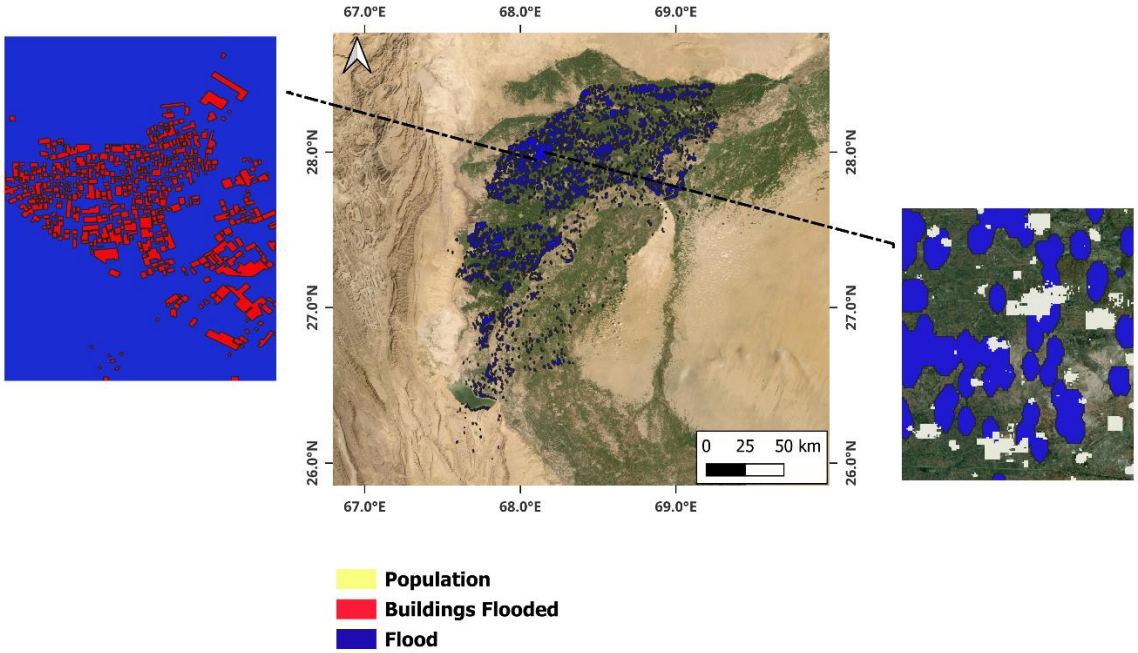


Figure 11: The final flood map is based on the SAR image for the year 2020, including an example of building exposure using the flood map and building data for Garhi Khairo municipality, and population exposure based on the flood mask and population data for Garhi Khairo municipality.

In contrast, the 2025 analysis shows that exposure percentages dropped a lot. The highest impact was in Kandhkot at 5.1%, followed by Gambat at 4.1% (Fig. 10(b)). These areas were labeled as "Minor affected". However, the municipality of Sijawal Junejo, which had one of the highest exposures in 2020, dropped to the lowest in 2025 with only 0.1%, Bhiria followed at 0.2%. This suggests that while flood risk still exists in the region, the severity of building exposure can change a lot depending on the flood scenario and the area.

There seems to be a correlation between flood hazard in the Garhi Khairo region and building exposure, both of which have been categorized as "Major affected". In contrast, the municipality of Kandhkot in 2025 exhibited a 51.7% flood hazard, also classified as “Major affected,” while building exposure was only 5.1%, categorized as “Minor affected” (Fig. 8 and 10). Further analysis revealed that Sijawal Junejo experienced a significant decrease in 2025, with both flood hazard (2.8%) and building exposure (0.1%) falling into the “Minor affected” category. In New Sukkur, building exposure was 3.7% (Fig. 10), which was substantially lower than the flood hazard percentage of 59.8% (Fig. 8). These findings suggest that although flood hazard and building exposure categories may align in certain cases, the severity percentages can differ considerably depending on infrastructure density. The average building exposure in the region is 1.9%.

4.5 Population Exposure:

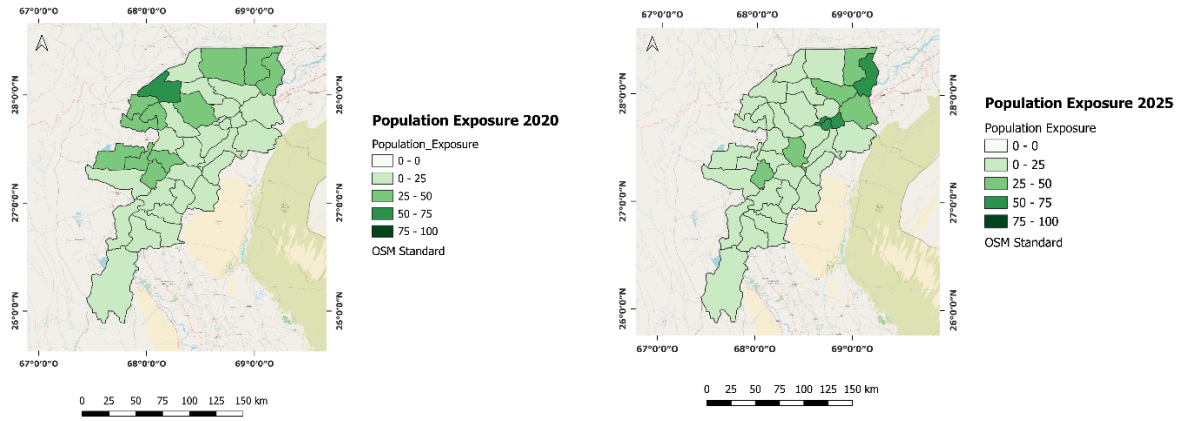
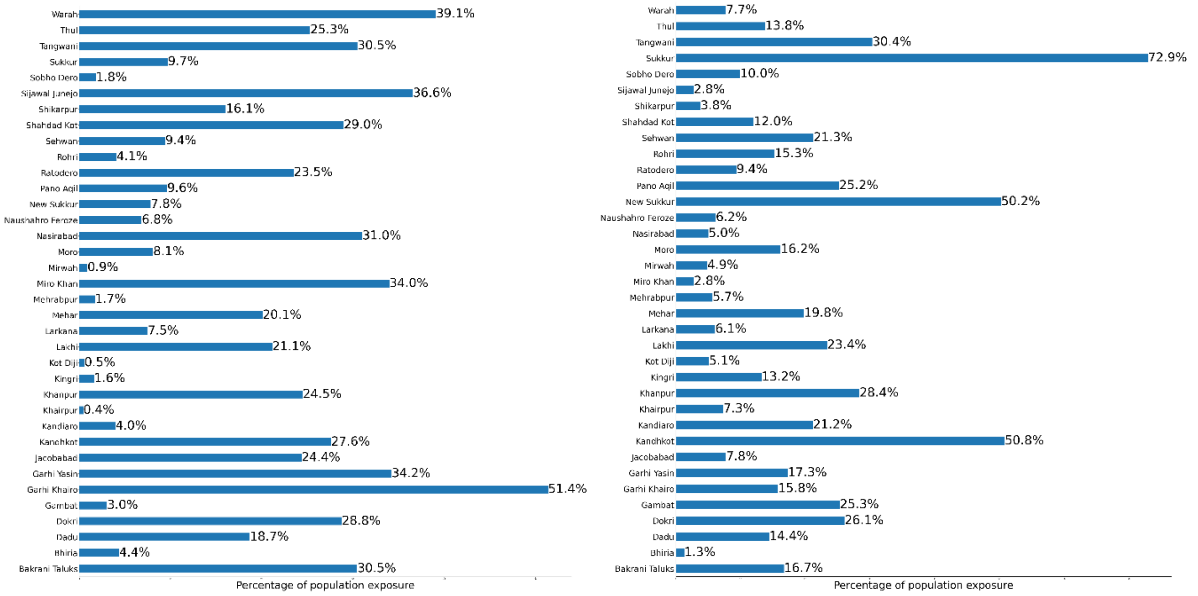


Figure 12: Population Exposure for the year 2020 (left) and 2025 (right).

We performed a population exposure analysis utilizing the WorldPop dataset, which offers high-resolution spatial distribution data. In order to analyze population exposure, we used the WorldPop dataset, which provides high-resolution spatial distribution data.



(a) (b)

Figure 13: Percentage of Population Exposure for the years 2020 (a) and 2025 (b).

Our analysis was based on overlaying the population map with the flooded pixel map (see Figs. 11 and 14), to determine the severity percentage of the affected population by using a zonal statistics approach. According to our research findings for the year 2020, Garhi Khairo is the municipality with the highest level of population exposure at 51.4%, while Warah is at 39.1% and Sijawal Junejo is at 36.6% (Fig. 13a). In Garhi Khairo, the population exposure is classified as “Major affected”, and in Warah and Sijawal Junejo, the population exposure is classified as “Affected”. However, Khairpur and Kot Diji were the least impacted municipalities, with exposure levels of only 0.4% and 0.5%, respectively, as shown in Figure 13a.

By 2025, population risk shifted noticeably, especially in the eastern region. Sukkur became the main hotspot, with population exposure increasing from 9.7% in 2020 to 72.9% in 2025 (Fig. 13a,b). Kandhkot also experienced a substantial rise in exposure, nearly doubling from 27.6% to 50.8%. New Sukkur's exposure increased from 7.8% to 50.2%.

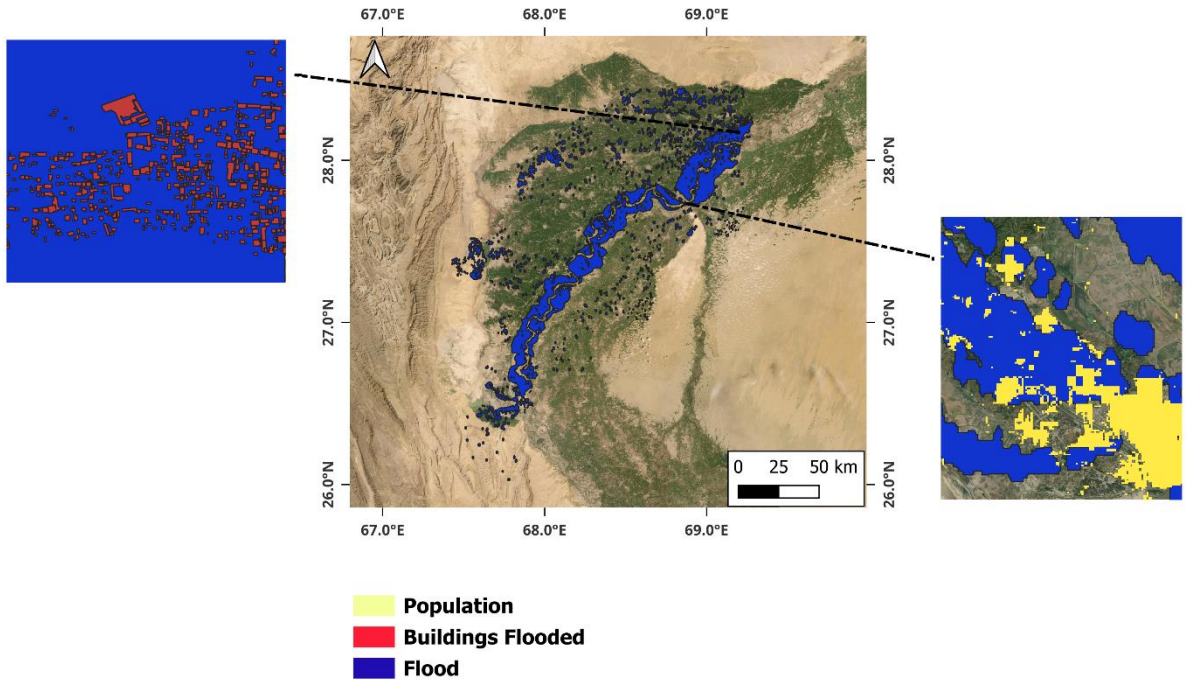


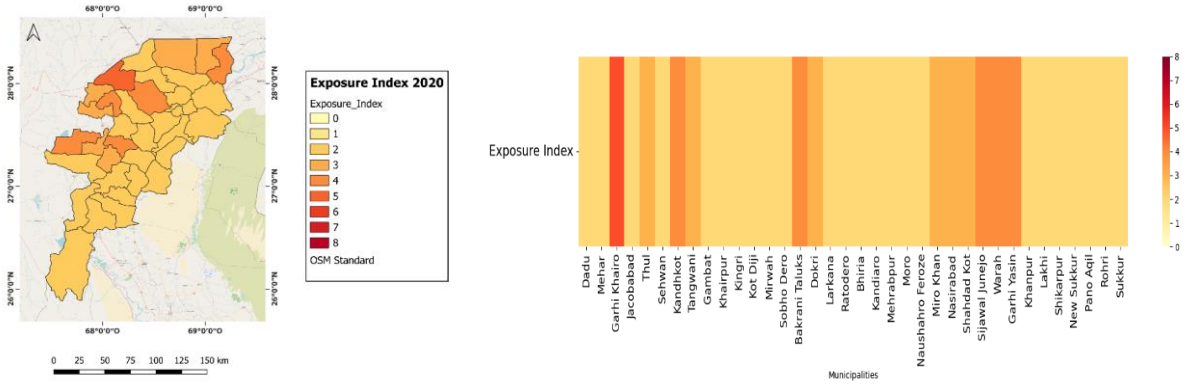
Figure 14: The final flood map is based on the SAR image for the year 2025, including an example of building exposure using the flood map and building data for Kandhkot municipality, and population exposure based on the flood mask and population data for Sukkur municipality.

All three municipalities moved into the "Major affected" category during this period. On the other hand, some municipalities that were high-risk in 2020 exhibited a substantial reduction in population exposure. Garhi Khairo, the most affected in 2020 with an exposure rate of 51.4%, declined to 15.8% by 2025. Sijawal Junejo also demonstrated a significant decrease, with exposure falling from 36.6% to 2.8%. Similarly, Miro Khan, which had an exposure rate of 34.0% in 2020, decreased to 2.8% by 2025 (Fig. 13a,b). Conversely, Bhiria remained mostly steady but had the lowest overall exposure in 2025 at 1.3%, down from 4.4% in 2020. The town of Dadu also showed a small decrease, going from 18.7% to 14.4%.

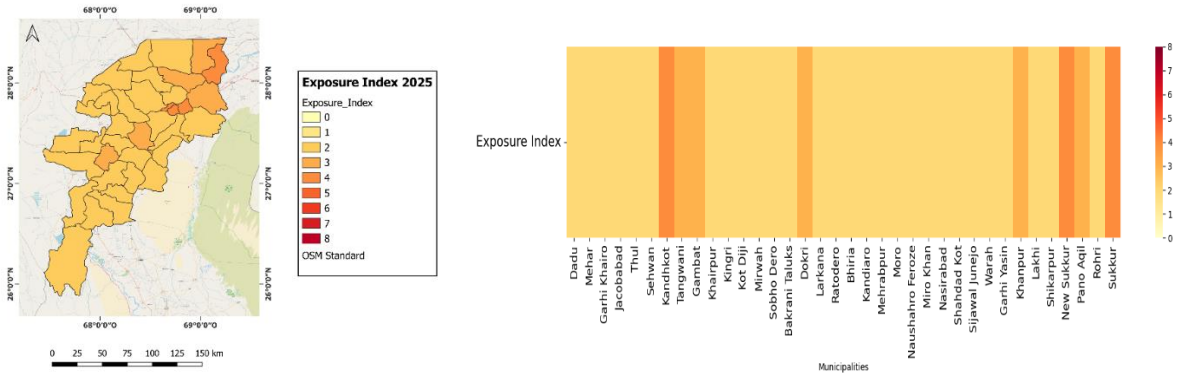
In the Garhi Khairo region in 2020, a strong correlation was identified between flood hazard (54.2%) and population exposure (51.4%), with both classified as "Major affected." In 2025, the municipality of Sukkur exhibited a 53.3% flood hazard and a substantially higher 72.9% population exposure, suggesting many people live in the flood-prone urban center. Further analysis revealed that New Sukkur also demonstrated a similar alignment, with both flood hazard (59.8%) and population exposure (50.2%) categorized as "Major affected." In Kandhkot, population exposure was 50.8%, almost the same as its flood hazard at 51.7% (Figs. 13b & 8). These findings suggest that while flood hazard and population exposure were

generally in the same categories, severity may increase in densely populated urban areas. Meaning that the population location plays a role in the exposure intensity. The average population exposure in the region for the 2025 scenario is 18.7%.

4.6 Exposure Index:



(a)



(b)

Figure 15: Exposure Index for the year 2020 (a) and 2025 (b).

Our study represents the results of an Exposure Index (EI) analysis developed to quantify the cumulative impact on both the built environment and local populations. The EI combines both building and population exposure across different administrative regions and provides a strategic metric for evaluating the cumulative resources needed during a flood. In the 2020 scenario, the municipality of Garhi Khairo exhibited the highest index value of 5/8 (Fig. 15a), indicating a primary need for resources after the flood. Other municipalities, including Thul, Kandhkot, Bakrani Taluks, Sijawal Junejo, and Garhi Yasin, showed moderate to high index values between 3/8 and 4/8 as represented in Figure 15a.

By 2025, we can observe a dramatic change in EI. The municipality of New Sukkur records the highest index value at 5/8, followed by Sukkur and Kandhkot, both with values of 4/8 (Fig. 15b). This pattern indicates that the demand for immediate assistance has shifted to these eastern urban centers. In contrast, municipalities such as Dadu, Mehar, Jacobabad, and Sijawal Junejo require very little assistance in 2025, with index values dropping to 1/8 or 2/8. The gap between these exposure indices can be due to several factors: The flood hazard may vary between events, with differences in flood intensity and flood extent maps. Population density may have changed over time.

It is important to note that the index values were calculated by taking into consideration the surface area, the population, and the number of buildings in each municipality. Even if two municipalities have similar index values, resources are allocated based on factors like building density and how many people live in each area. These findings show that, although the average EI varies, the severity in specific locations leads to important changes in how disaster mitigation and resources are managed in each region.

4.7 Vulnerability:

4.7.1 Gross Domestic Product (GDP):

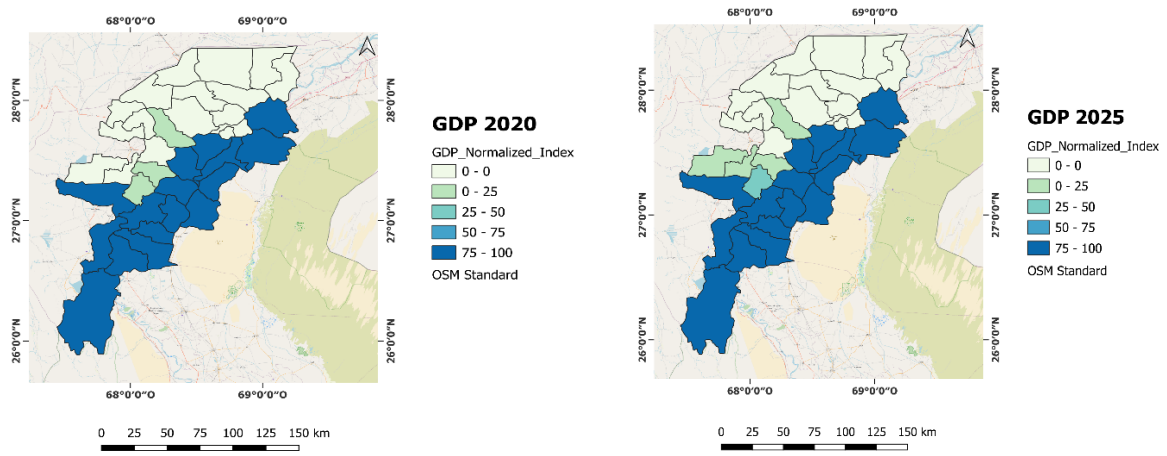


Figure 16: Normalized GDP per Capita (PPP) for the year 2020 (left) and 2025 (right).

The map in Figure 16 shows the variation in the normalized GDP per capita (PPP) index in 2020 and 2025 for the northern municipalities of Sindh. To assess the socio-economic conditions of the people, GDP per capita (PPP) was added as a socio-economic indicator and was integrated into the vulnerability assessment. Due to the absence of economic data at the municipal level (Adm level 3), GDP was assessed at the district level (Adm level 2). All the

original GDP per capita values were rescaled to a 0–100 scale for comparison with the other indicators in the flood risk framework.

The results show a clear difference in economic conditions within the study regions. Overall, the normalized GDP per capita values were higher in the municipalities of the southern and central parts of the region in both 2020 and 2025, whereas several municipalities in the north had comparatively low values. The pattern suggests that there may be variations in economic capacity between municipalities, and therefore in their preparedness, response, and recovery from flood events. When these results are compared to the flood hazard maps (Figure 7), some significant differences between the location of the most severe flood hazards and economic conditions can be seen. In 2020, several municipalities in the northern part of the study area, such as Garhi Khairo, Shahdad Kot, and its surrounding municipalities have relatively high flood hazard and low GDP per capita index value. This combination indicates a high socio-economic vulnerability, as a population that are more vulnerable to flooding might have limited socio-economic resources to recover from and adapt to flooding.

The flood hazard pattern changed in 2025, moving to a few municipalities having moderate to higher GDP per capita. It can be seen that, high flood hazard was observed in municipalities with higher GDP per capita, including New Sukkur and Sukkur. This demonstrates a shift of the flood effects from mainly lower-income municipalities to more economically developed municipalities. It is important to note that physical flood hazard and socio-economic factors must be taken into account when assessing flood vulnerability and risk.

4.7.2 Poverty Rate:

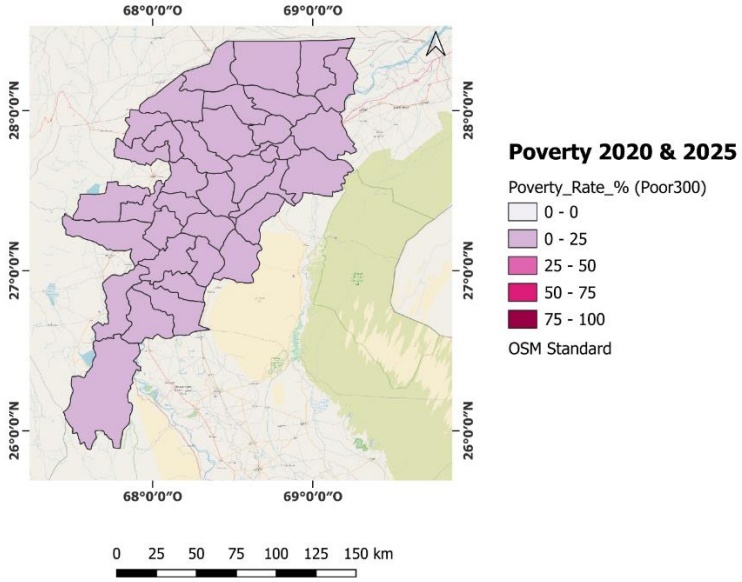


Figure 17: Poverty rate for the years 2020 and 2025.

Poverty is a major factor of flood vulnerability as those who are poor have less ability to prepare for, respond to, and recover from flood events. Many previous studies have confirmed that the effects of a flood can be exacerbated by poverty, as it can reduce the availability of resources, infrastructure, and recovery capabilities, thereby increasing exposure to the effects of the disaster (Rentschler et al., 2022). So, in this study, poverty was used as a social vulnerability indicator and was interpreted along with flood hazard information.

Poverty data were downloaded from the World Bank Geospatial Poverty Portal based on the poverty rate at $3.00 per person per day (2021 PPP). The poverty rate was reported as 18.58% for Sindh Province and applied across all municipal levels, as there was no data on poverty at the municipal level for this province. To ensure consistency within the integrated index, this value was normalized on a 0–100 scale. This value was applied as a constant across all municipalities for both the 2020 and 2025 scenarios. Although it does not vary throughout the study area, it provides valuable information on the vulnerability of people who are exposed to flood hazards. In regions with high poverty rate and high flood hazards, affected communities are more vulnerable as they may experience more difficulties in flood recovery and adaptation.

4.7.3 Gini Coefficient:

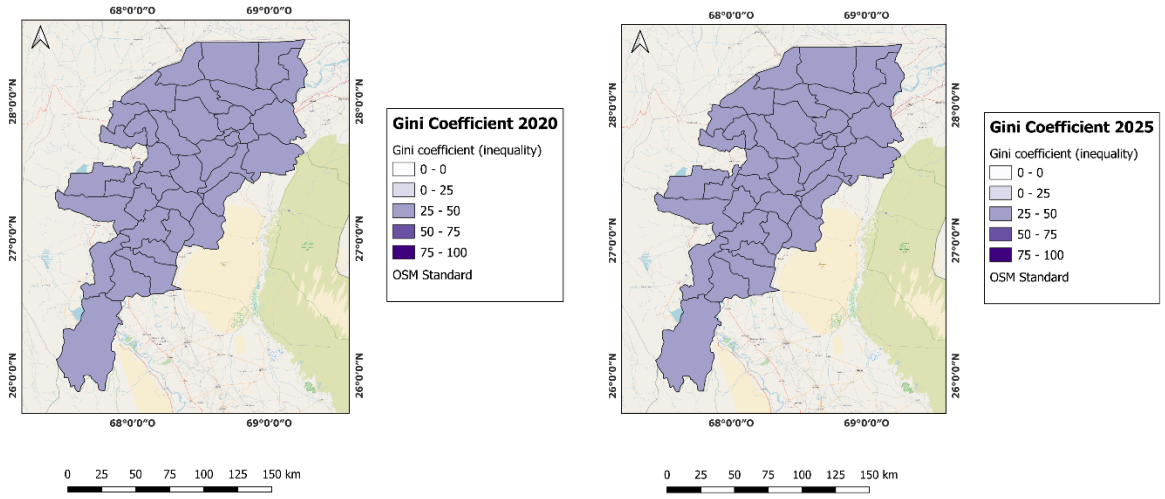


Figure 18: Gini Coefficient for the year 2020 (left) and 2025 (right).

The Gini coefficient is a widely used way to measure income inequality in a population. Higher values suggest a more unequal distribution of income, while lower values suggest a more equal distribution of income (World Bank, 2024). To represent income inequality throughout the study area, the Gini coefficient was used in this study. In our study, we utilized the Gini coefficient to measure the wealth gap, which can limit access to private resources during an emergency. For 2020 and 2025, there were no detailed municipal-level data (Adm level 3) available, so we used provincial-level data (Adm level 1) in their place. The Gini coefficient was recorded as 0.384 in 2020 and 0.383 in 2025. For the purpose of maintaining consistency within the integrated index, these values have been normalized to 38.4 and 38.3, respectively, on a 0–100 scale. These normalized figures were applied as constants throughout all municipalities for both 2020 and 2025. This coefficient illustrates the effects of income inequality on people's ability to recover from disasters, making it an important part of the Vulnerability Index.

4.7.4 Human Development Index (HDI):

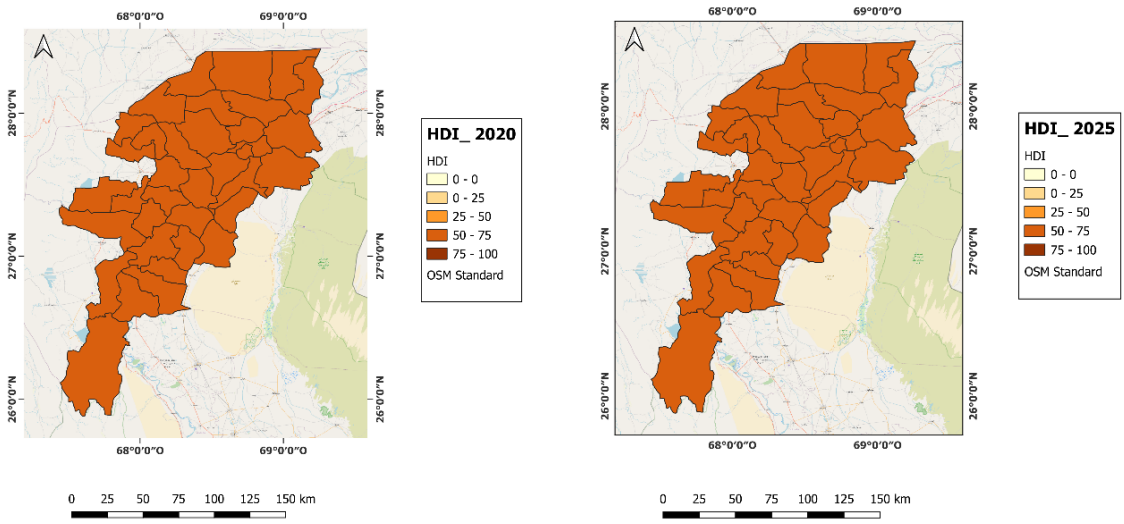
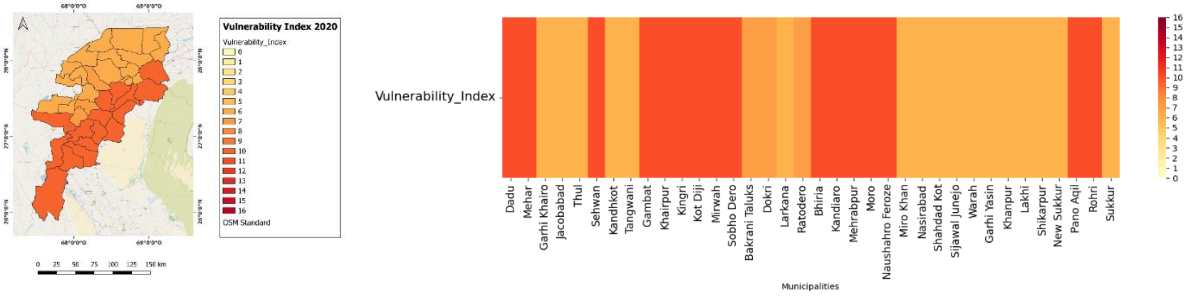


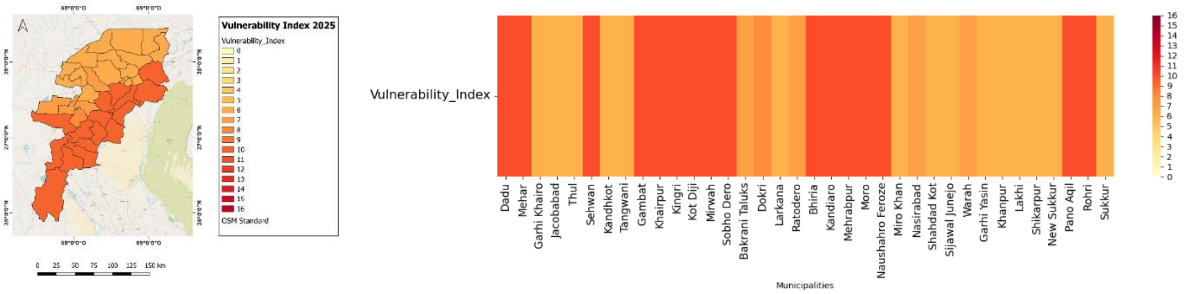
Figure 19: HDI for the year 2020 (left) and 2025 (right).

The Human Development Index (HDI) is a broad assessment of how well a community can adapt, utilizing health, education, and living standards to illustrate its ability to handle environmental problems/challenges (UNDP, 1990; Birkmann et al., 2013). In this analysis, we employed provincial-level data because complete HDI data were not available at the municipal level (Adm level 3). In 2020, the HDI was 0.509, normalized to 50.9 on a 0–100 scale. By 2025, the HDI increased significantly to 0.514, normalized to 51.4. We used these numbers as regional constants across all municipalities for each year to produce a consistent measure of the population's well-being and its ability to cope with flood hazards.

4.5 Vulnerability Index:



(a)

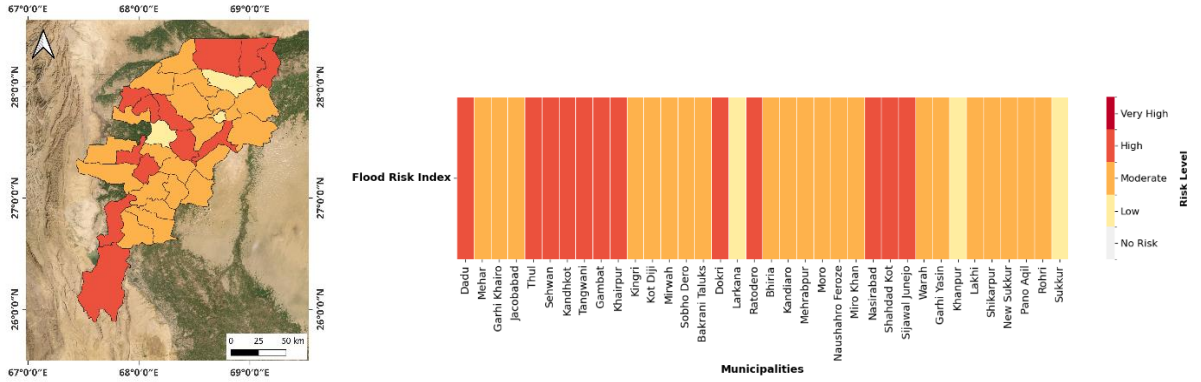


(b)

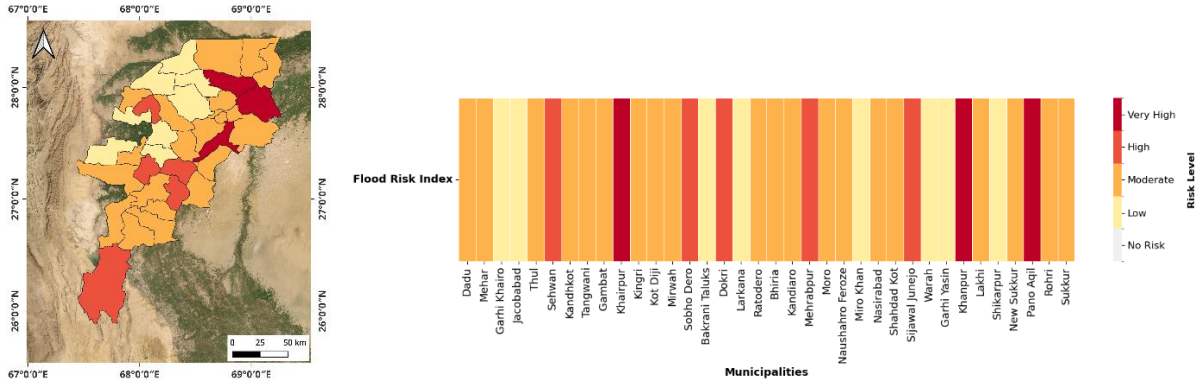
Figure 20: Vulnerability Index for the year 2020 (a) and 2025 (b).

Our study represents the results of the Vulnerability Index (VI) for 2020 and 2025, illustrating how the different places in the region are to encounter disasters. It integrated data of GDP, the Gini Coefficient, the Human Development Index (HDI), and poverty rates. As for the GDP and poverty explanations, we would like to better understand the Gini coefficient, especially in the areas affected by the flood. Based on the IPCC (2014) framework, these indicators collectively help estimate how well individuals can adapt and how unstable their structures are. Although the vulnerability Index has scales from 0 to 16, the observed values in the research area ranged from 6 to 10. In both the 2020 and 2025 scenarios, several municipalities such as Dadu, Sehwan, Khairpur, Naushahro Feroze, and Rohri exhibited the highest index value of 10/16 (Fig. 20a), indicating a serious combination of high economic risk and low adaptability. As we move to only 2025, however, vulnerability has increased in some municipalities, including Dokri from 7 to 8; Warah and Nasirabad from 6 to 7 as represented in Figure 20b. During both years, municipalities like Kandhkot, Larkana, and Sukkur maintained a consistent score of 6.

4.6 Flood Risk Assessment:



(a)



(b)

Figure 21: Flood Risk Map for the year 2020 (a) and 2025 (b).

The Flood Risk Index, which combines hazard, exposure, and vulnerability, measures overall disaster risk across the study area, ranging from no risk to very high risk. It is observed from the graph that in 2020, risk levels were clearly high in 12 municipalities, including Dadu, Thul, Sehwan, Kandhkot, Tangwani, Gambat, Khairpur, Dokri, Ratodero, Nasirabad, Shahdad Kot, and Sijawal Junejo, while several north-western and south-eastern regions remained in the moderate-risk category. On the other hand, municipalities such as Larkana, Khanpur, and Sukkur show a low risk.

There is evidence that by 2025, the risk has increased sharply and shifted away from the western areas to the eastern areas. Khanpur, Pano Aqil, and Khairpur became the main regional hotspots, reaching the highest risk level. This rise is most clear in towns that jumped quickly in risk category; specifically, Pano Aqil went from moderate risk to very high risk, Khanpur from low

risk to very high risk, and Khairpur from high risk to very high risk. There was, however, a noticeable reduction in flood risk in some municipalities, even if the overall trend was toward increasing risk. A good example of this is Kashmore, Tangwani, and Kandhkot, which were all in the high-risk group in 2020, but they have shifted to the moderate-risk group in 2025, indicating a notable improvement in their risk status during this time period. It is essential to point out that the risk category for Gari Khairo and Jacobabad has changed from moderate to low, indicating that the vulnerability of the two areas has further decreased.

Chapter 5:

5 Discussion and Conclusion

5.1 Framework Contribution:

In this study, we assessed the Impact of floods Utilizing Satellite data in the Northern regions of Sindh province, Pakistan. This present study has designed an integrated rapid flood-risk assessment framework based upon freely available satellite imagery and socio-economic datasets, which assesses flood hazard, exposure, vulnerability, and overall flood risk in the selected study regions. The aim of this research is to develop a rapid and accurate assessment framework, which can be applied throughout the world, especially in low and low-middle-income countries: data-scarce regions, where detailed monitoring systems and field-based observations are often unavailable. The framework adopted a quantitative risk assessment approach that combined Hazard, Exposure, and Vulnerability components in the standard flood risk equation (Risk = Hazard × Exposure × Vulnerability), this integrated approach is based on the conceptual framework for flood risk developed in the IPCC, which states that disaster risk is the product of hazard, exposure, and vulnerability (IPCC, 2014).

This study demonstrates that a consistent satellite-based workflow utilizing Sentinel-1 Synthetic Aperture Radar (SAR) is essential for rapid mapping. For the flood event mapping, we employed data as the primary source from Sentinel-1 SAR, which enables observations just near the peak of a flooding event regardless of weather conditions, even in cloudy conditions.

A key strength of Sentinel-1 SAR is its ability to view through clouds, which markedly accelerates and increases the reliability of rapid flood assessment, where optical imagery (e.g., Sentinel-2, Landsat) is often blocked during extreme weather events. This finding aligns with the study by Schumann and Moller (2015), who noted that during severe weather conditions, optical imagery can often be obscured, and hence the SAR systems are highly effective for operational monitoring of floods. Their study also confirmed that SAR-based flood mapping provides reliable information in near real-time, to support emergency response and disaster management.

When we compare the methods that we used for mapping flood areas to the CEMS rapid mapping methods, we find that they provide a quick, easy, and accurate approach to mapping flood areas, supporting more effective decision-making during flood emergencies (Schumann & Moller, 2015).

For validation, we used data from Sentinel-2 and Landsat 8 to calculate the Normalized Difference Water Index (NDWI), to create the most accurate and reliable flood map, and deliver an accurate flood risk index assessment. This combination of SAR for detection and optical imaging for validation increases confidence in flood maps and enables more informed allocation of emergency resources. The same approach was employed by Tran et al. (2022) in the Mekong Delta, where Sentinel-1 SAR imagery was integrated with NDWI-based optical validation. They concluded that the integration of SAR and optical data is very effective for flood detection. They also highlighted in their research that SAR-based thresholding techniques work well for the rapid flood mapping in large floodplain areas.

5.2 Thresholding Performance:

In our analysis, a major goal was to evaluate or assess the effectiveness of several thresholding techniques for Sentinel-1 SAR-based flood mapping. We employed four different thresholding methods, including Otsu (Jianzhuang et al., 1991), Triangle (Zack et al., 1977), Standard Deviation (Li & Liu, 2009), and Threshold Minimum (Prewitt & Mendelsohn, 1966), compared using Sentinel-1 SAR images acquired before and after the disaster in the study region. In this study, we find that thresholding performance is strongly influenced by SAR Digital Number (DN) distributions and land-cover characteristics. Therefore, the selection of an optimal thresholding technique for the single event entirely relies on the pixel intensity distribution.

During the 2025 flood event, the Standard Deviation method performed best. This is because the DN values followed a clear Gaussian distribution and were close to a normal distribution. In this case, water pixels grouped around a distinct low-backscatter range allowed separating water pixels from land, and distinguishing flooded and non-flooded areas. Similar findings were reported by Li and Liu (2009), who found that the standard deviation thresholding method is suitable when the image histograms are close to normal distributions.

In contrast, by 2020 event, the Otsu thresholding method was more accurate. This is probably because the DN histograms were more irregular, as a result of complex land-cover interactions, such as vegetation, wet soils, and urban backscatter effects. Otsu thresholding is more appropriate for heterogeneous flood environments, and it handles irregular histograms better. A similar observation was reported by Martinis et al. (2009). According to their findings, adaptive thresholding performs better than others for detecting floods in heterogeneous landscapes. Additionally, these findings align with Liang et al. (2020), who indicated that there is no single thresholding method for all flood detection, since SAR backscatter values vary depending on

topography, vegetation, urban structures, and water conditions. In urban locations, reflections from infrastructures and roads can make water harder to detect, whereas in densely vegetated regions, in areas with lots of plants, flooded ground can be hidden under the leaves.

The study demonstrates that testing various thresholding techniques is crucial for enhancing the accuracy of SAR-based flood classification and also indicates that the choice of thresholds is rather event-specific. By selecting the most suitable threshold for each image, we produced the most reliable final flood masks.

5.3 Comparison of Flood Hazard Between 2020 and 2025:

Comparing the 2020 and 2025 flood events reveals clear differences in where and when floods occur. Creating a flooded-area map allows us to determine hazard intensity based on the flood hazard. The findings show an increase in average flood hazard from 20.4% in 2020 to 25.2% in 2025, showing floods are getting worse overall. There was also a shift in flood hotspots, moving from western municipalities to eastern urban centers, like the municipalities of Garhi Khairo and Shahdad Kot, which were the most affected by the 2020 flood hazard, with 54.2% and 47.3%, whereas in 2025, risk levels increased sharply in the eastern and northern areas, with New Sukkur reaching a peak of 59.8% hazard, followed by Sukkur at 53.3% and Kandhkot at 51.7%. These changes could be due to factors like hydrological variability, changes in land use, or the wider effects of climate change. A similar observation was reported by IPCC (2014), which noted that climate change is leading to a rise in the number of extreme hydrological events occurring around the world, particularly in the vulnerable developing regions. Rapid urbanization, in some cases, can increase flood hazard by decreasing infiltration and increasing surface runoff. Similarly, a key concern in urban flood expansion in developing areas is that drainage planning is often lacking as infrastructure grows (Du et al., 2015).

A high proportion of flood hazard in urban municipalities is particularly significant due to higher population densities, infrastructure density, and economic value (Winsemius et al., 2016). Therefore, the socio-economic impacts of flood extents may be disproportionately high in urban areas compared to rural areas, even if the flood extent is relatively small. The same has been stated by Jha et al. (2012) who pointed out that urban flooding may cause more economic loss due to concentration of infrastructure, high population density and poor drainage infrastructure.

5.4 Exposure Analysis and Exposure Index (EI):

One of the important findings of this study is that there is no direct relationship between flood hazard and the intensity of exposure. Some municipalities saw a large amount of flood water, but relatively low exposure to buildings, while others had a high population exposure because the flood water reached high in a densely populated residential area. For example, by the 2025 event, Kandhkot faced a flood hazard of over 50%, but the number of exposed buildings stayed fairly low. In contrast, Sukkur shows a higher number of populations exposed (more than 70%), even though the hazard level was relatively low. This means that floodwaters reached densely populated residential areas. Similarly, these also show that the effects of flooding are heavily dependent on the allocation of land use, infrastructure and population rather than just the extent of flooding. Kreibich et al., 2022, also reached similar results including the importance of socio-spatial patterns for flood impacts.

To assess the exposure to flood, the Exposure Index (EI) was developed using both population and building data. This EI can be useful for better understanding resource demand during flood events. The trend of high EI values moving towards the urban municipalities indicates increased flood sensitivity in urban areas. The findings in this study agree with the findings of Douglas et al. (2008) who concluded that urban regions are highly exposed to flood disasters because of the high concentration of population and infrastructure.

The EI can help make quick decisions and plan emergency responses by identifying municipalities that need more help and resources after disasters. The combination of flood hazard data and exposure indicators improve disaster management planning, resource allocation and adaptation to climate change, particularly in developing countries that have limited ability to do on-site assessments.

5.5 Vulnerability Analysis and Vulnerability Index (VI):

The Vulnerability Index (VI) was calculated through the integration of GDP, poverty rate, Gini coefficient, and Human Development Index (HDI) datasets to assess adaptive capacity and socio-economic sensitivity of populations of the study area. The municipalities of Dadu, Sehwan, Khairpur and Rohri were found as vulnerable municipalities, because they had a high level of economic value and a low level of adaptability.

Based on these findings, it can be concluded that even if a municipality has a high level of economic involvement, high impacts of disasters may occur if social resiliency and recovery

capacity is low. According to Birkmann et al. (2013), vulnerability is multidimensional and is significantly influenced by economic, social, and institutional factors. Similarly, the Human Development framework developed by the United Nations Development Programme (UNDP) also highlights that the education, health and living standards of communities are inversely linked to their ability to recover from environmental disasters.

On the other hand, less developed northwestern regions, while still exposed to hazards, usually face lower losses. Vulnerability levels stay mostly the same from 2020 to 2025, but their effect on overall risk grows in 2025 as more people are exposed, especially in urban areas. This shows that vulnerability is a key factor that shapes both the severity of flood impacts and how well communities can respond and recover (Adger, 2006).

5.6 Flood Risk Index Assessment:

The final Flood Risk Index enabled a clearer understanding of flood risk between the 2020 and 2025 flood events in the study area by bringing together hazard, exposure, and vulnerability into a single framework. In 2020, the municipalities in the western part of the country, including Dadu, Sehwan, Kandhkot, and Shahdad Kot were mostly at higher risk of flooding. The top risk was transferred to the eastern regions, including Khanpur, Pano Aqil and Khairpur by 2025. The pattern of flood risk has changed significantly between the two years. The increase in risk in the eastern municipalities could be related to higher population and urban development. Some municipalities, however, experienced a reduced overall flood risk despite being at risk from flooding.

The results show that the overall flood risk depends not only on the flood extent but also on the flood exposure and socio-economic vulnerability conditions. Meaning that a flood can be hazardous, but the exposure and vulnerability are not, the overall flood risk may remain low if the exposure and vulnerability are not high. Birkmann et al. (2013) also reached similar conclusions, stating that disaster risk is the combined interaction of hazard, exposure, and vulnerability. The results also indicate that flood-risk assessment is more realistic than flood hazard mapping in understanding the impacts of flood disasters. Moderate flood hazard areas could have a greater overall risk if they have vulnerable populations located in floodplains and exposed infrastructure. Similar to this, Devitt et al. (2022) and Rogers et al. (2025) also pointed out that socio-spatial aspects (population distribution, urban concentration, and socio-economic conditions) are important determinants of flood-risk patterns.

The Flood Risk Index created in this study allows for a rapid evaluation of flood risk, emergency response planning and the allocation of resources by providing information on which municipalities require the greatest help after a disaster. This is especially useful during major floods, when on-the-ground assessments / field-based assessments are sometimes challenging due to infrastructure damage, a lack of personnel, and limited accessibility to the field for rapid assessment. In such cases, free publicly available satellite imagery and open socio-economic data can provide an efficient, affordable, and time-effective solution for rapid assessment of the flood impacts and prioritize the location of emergency response activities. The proposed framework would help governments, disaster management organizations, agencies, NGOs, and humanitarian groups to identify the most affected regions and allocate resources more efficiently when the floods occur. This method is based on data from the entire globe and a set of repeatable steps, making it suitable for application in other parts of the world, particularly data-scarce developing countries that are prone to flooding, where detailed monitoring and disaster records are not available.

5.7 Sustainable Development Goal (SDG) Implications:

The proposed framework has shown a good alignment to the Sustainable Development Goal (SDG) 11 on cities and communities, the target of which is to build inclusive, safe, resilient, and sustainable cities and communities. The framework can be applied to identify and assess the high risk of flooding in particular municipalities, which will then inform urban planning, disaster preparedness, and building resilient urban infrastructure, particularly in flood-prone areas. Also, the United Nations Sendai Framework for Disaster Risk Reduction emphasizes disaster preparedness, resilience, and planning for risk awareness.

The framework also indirectly supports SDG13 (Climate Action) through climate risk assessment and climate adaptation planning for flood-related disasters. Combining hazard, exposure, and vulnerability into one framework provides a better understanding of the impacts of floods and facilitates long-term climate risk adaptation planning. The Intergovernmental Panel on Climate Change (IPCC) has also suggested similar strategies to enhance climate resilience and disaster risk reduction.

5.8 Limitations and Future Research:

Although the framework has been found helpful for rapid flood risk assessment, it does have some limitations. First, the revisit times of the satellites (Sentinel-1, Sentinel-2, and Landsat 8). The framework does not work well for monitoring flash floods because of differences in the revisit times of Sentinel-1, Sentinel-2, and Landsat 8, and the time periods of the flood events. There is a 12-day revisit time for Sentinel-1 (Nava et al., 2024). If there is a considerable gap between satellite observations, a significant amount of information or changes in the flood situation may not be captured, which means the flood hazard, building exposures, and population exposures could be underestimated near the peak of the flood.

Second, implementing this framework in cities can be difficult. However, using Sentinel-1 (SAR) data in urban areas is challenging, mainly because of the reflectance of buildings and mixed land-cover surfaces, which might reduce the accuracy of flooded area mapping in highly developed urban areas.

Another key limitation is that detailed high-resolution socio-economic data were not available at the municipal level. Some of the socio-economic indicators calculated for the Vulnerability Index, such as the poverty rate, the Gini coefficient, and HDI, are available only at the province (ADM-1) level and not at the municipality level. These values were then normalized and used as constants in the analysis. This meant that these indicators were applied to the whole municipality and therefore did not capture the local variations of the vulnerability analysis.

Further studies are needed to combine SAR and optical data at higher resolutions, as well as other higher spatial resolution data from advanced sensors (TerraSAR-X, TanDEM-X, and WorldView imagery), to enhance flood mapping accuracy in flash flood and urban areas. The hydrologic and meteorological parameters like flood depth, rainfall intensity, runoff, and water velocity were also included, which could further enhance the assessments of flood risk and flood damage. Machine-learning and deep-learning methods for automated flood mapping and a more detailed exposure analysis could also be explored in future research. In addition, the creation of the socio-economic data sets at the municipality level would enhance vulnerability assessment and help to make better planning and allocation for disaster management.

Bibliography:

Adger, W. N. (2006). *Vulnerability*. Global Environmental Change, 16(3), 268–281. https://doi.org/10.1016/j.gloenvcha.2006.02.006

Asian Development Bank (ADB). (2021**).** Climate Risk Country Profile: Pakistan.

Birkmann, J., Cardona, O. D., Carreño, M. L., Barbat, A. H., Pelling, M., Schneiderbauer, S., ... & Welle, T. (2013). Framing vulnerability, risk and societal responses: The MOVE framework. *Natural Hazards*, 67(2), 193–211. https://doi.org/10.1007/s11069-013-0558-5

Biswas, B., Ghute, B., & Das, J. (Eds.). (2025). Geoinformatics for Flood Risk Management: Applications and Strategies (1st ed.). CRC Press. https://doi.org/10.1201/9781003533511

Chrisendo, D., Niva, V., Hoffmann, R., Sayyar, S.M., Rocha, J.C., Sandström, V., Solt, F., & Kummu, M. (2025). *Rising income inequality across half of global population and socioecological implications*. Nature Sustainability. https://doi.org/10.1038/s41893-025-01689-4

Cutter, S. L., Boruff, B. J., & Shirley, W. L. (2003). Social vulnerability to environmental hazards. *Social Science Quarterly*, 84(2), 242–261. https://doi.org/10.1111/1540-6237.8402002

Devitt, L., Neal, J., Coxon, G. Savage. J & Wagener. T (2023). Flood hazard potential reveals global floodplain settlement patterns. *Nat Commun* **14**, 2801. https://doi.org/10.1038/s41467-023-38297-9

Du, S., Shi, P., Van Rompaey, A., & Wen, J. (2015). Quantifying the impact of impervious surface location on flood peak discharge in urban areas. Natural Hazards, 76, 1457–1471.

eoPortal. (2018, November 8). *Copernicus: Sentinel-2—The optical imaging mission for land services*. Copernicus. https://directory.eoportal.org/web/eoportal/satellite-missions/c-missions/copernicus-sentinel-2

Eudaric, J., Kreibich, H., Camero, A. *et al.* A satellite imagery-driven framework for rapid resource allocation in flood scenarios to enhance loss and damage fund

effectiveness. *Sci Rep* **14**, 19290 (2024). https://doi.org/10.1038/s41598-024-69977-1

Food and Agriculture Organization of the United Nations (FAO). (2020). *Pakistan monsoon floods situation report 2020.*

Giustarini, L., Hostache, R., Matgen, P., Schumann, G. J. P., Bates, P. D., & Mason, D. C. (2015). A change detection approach to flood mapping in urban areas using TerraSAR-X. *IEEE Transactions on Geoscience and Remote Sensing*, 53(3), 1538–1552. https://doi.org/10.1109/TGRS.2014.2340125

Global Data Lab. (2024). Subnational Human Development Index (SHDI) database. Institute for Management Research, Radboud University. https://globaldatalab.org/shdi/

Government of Pakistan (2023). *Pakistan Economic Survey 2022–2023*. Ministry of Finance, Islamabad.

He, K., Yang, Q., Shen, X., Dimitriou, E., Mentzafou, A., Papadaki, C., Stoumboudi, M., and Anagnostou, E. N. (2024): Brief communication: Storm Daniel flood impact in Greece in 2023: mapping crop and livestock exposure from synthetic-aperture radar (SAR), Nat. Hazards Earth Syst. Sci., 24, 2375–2382, https://doi.org/10.5194/nhess-24-2375-2024.

IPCC. (2014). Climate Change 2014: Impacts, Adaptation, and Vulnerability. Contribution of Working Group II to the Fifth Assessment Report of the Intergovernmental Panel on Climate Change. Cambridge University Press.

IPCC. (2022). Climate Change 2022: Impacts, Adaptation and Vulnerability. Contribution of Working Group II to the Sixth Assessment Report of the Intergovernmental Panel on Climate Change. Cambridge University Press. https://doi.org/10.1017/9781009325844

Jha, A. K., Bloch, R., & Lamond, J. (2012). Cities and Flooding: A Guide to Integrated Urban Flood Risk Management for the 21st Century. World Bank.

Jianzhuang, L., Wenqing, L., & Yupeng, T. (1991). Automatic thresholding of gray-level pictures using two-dimension Otsu method. *1991 International Conference on Circuits and Systems*. https://doi.org/10.1109/ciccas.1991.184351

Kreibich, H., Di Baldassarre, G., Vorogushyn, S., Aerts, J. C. J. H., Arnbjerg-Nielsen, K., Aronica, G. T., ... & Merz, B. (2022). Adaptation to flood risk: Results, challenges and future directions. *Natural Hazards and Earth System Sciences*, 22, 1683–1727. https://doi.org/10.5194/nhess-22-1683-2022

Kummu, M., Niva, V., Chrisendo, D., Rocha, J.C., Hoffmann, R., Sandström, V., Solt, F., & Masoumzadeh Sayyar, S. (2025). Global subnational Gini coefficient (income inequality) and gross national income (GNI) per capita PPP datasets for 1990–2023 [Data set]. Zenodo. https://doi.org/10.5281/zenodo.16410778

Kummu, M., Taka, M., Persson, L. (2025). Downscaled gridded global dataset for Gross Domestic Product (GDP) per capita at purchasing power parity (PPP) over 1990–2022. Scientific Data, 12, 567.

Li, Z., & Liu, C. (2009). An image thresholding method based on standard deviation. 2009 International Joint Conference on Computational Sciences and Optimization. https://doi.org/10.1109/cso.2009.177

Martinis, S., Twele, A., & Voigt, S. (2009). Towards operational near real-time flood detection using a split-based automatic thresholding procedure on high-resolution TerraSAR-X data. *Natural Hazards and Earth System Sciences*, 9(2), 303–314. https://doi.org/10.5194/nhess-9-303-2009

McFeeters, S. K. (1996). The use of the Normalized Difference Water Index (NDWI) in the delineation of open water features. *International Journal of Remote Sensing*, 17(7), 1425–1432. https://doi.org/10.1080/01431169608948714

Microsoft (2022). *Building Footprints*. https://www.microsoft.com/en-us/maps/building-footprints (2022)

National Disaster Management Authority (NDMA) (2023). Pakistan Flood Response and Recovery Report. Islamabad, Pakistan.

National Disaster Management Authority (NDMA). (2020). *Monsoon 2020 flood situation reports.*

Nava, L., Tordesillas, A., Qian, G., & Catani, F. (2024). Displacement residuals reveal landslide regime shifts. https://doi.org/10.1007/s10346-024-02353-2

Prewitt, J. M. S., & Mendelsohn, M. L. (1966). The analysis of cell images. *Annals of the New York Academy of Sciences, 128*(3), 1035–1053. https://doi.org/10.1111/j.1749-6632.1965.tb11715.x

Rahman, A. & Shaw, R. (2015). Flood risk, vulnerability and adaptation in Bangladesh and Pakistan river basins. In: Flood Risk Management. Springer.

Rahman, A., & Shaw, R. (2015). Flood risk, vulnerability and adaptation in South Asia. In R. Shaw (Ed.), *Disaster Risk Reduction Approaches in South Asia* (pp. 35–52). Springer.

Rentschler, J., Salhab, M. & Jafino, B.A (2022). Flood exposure and poverty in 188 countries. Nat Commun 13, 3527 (2022). https://doi.org/10.1038/s41467-022-30727-4

Rogers, J.S., Maneta, M.P., Sain, S.R. *et al.* (2025). The role of climate and population change in global flood exposure and vulnerability. *Nat Commun* **16**, 1287. https://doi.org/10.1038/s41467-025-56654-8

Schumann, G. J. P., & Di Baldassarre, G. (2010). The direct use of radar satellites for event-specific flood risk mapping. *Remote Sensing Letters*, 1(2), 75–84. https://doi.org/10.1080/01431161.2010.531783

Schumann, G. J.-P., & Moller, D. K. (2015). Microwave remote sensing of flood inundation. *Physics and Chemistry of the Earth*, 83–84, 84–95.

Smits, J., & Permanyer, I. (2019). *The Subnational Human Development Database*. Scientific Data, 6, 190038. https://doi.org/10.1038/sdata.2019.38

Synthetic Aperture Radar (2019). https://www.earthdata.nasa.gov/learn/backgrounders/what-is-sar.

Tatem, A. J (2017). Worldpop, open data for spatial demography. *Sci. Data* https://doi.org/10.1038/sdata.2017.4

Tran, K. H., Menenti, M. & Jia, L (2022). Surface water mapping and flood monitoring in the Mekong delta using sentinel-1 SAR time series and OTSU threshold. Remote Sens. 14, 2072–4292. https://doi.org/10.3390/rs14225721.

Twele, A., Cao, W., Plank, S., & Martinis, S. (2016). Sentinel-1-based flood mapping: A fully automated processing chain. *International Journal of Remote Sensing*, 37(13), 2990–3004. https://doi.org/10.1080/01431161.2016.1192304

UNDP (1990). Human Development Report 1990: *Concept and Measurement of Human*

United Nations Office for Disaster Risk Reduction (UNDRR). (2023). *Global Assessment Report on Disaster Risk Reduction 2023*. Geneva, Switzerland.

United Nations Office for the Coordination of Humanitarian Affairs (UNOCHA). (2025). *Pakistan floods situation report 2025.*

United Nations. (2015). Transforming Our World: The 2030 Agenda for Sustainable Development. United Nations, New York.

Winsemius, H. C., Aerts, J. C. J. H., van Beek, L. P. H., Bierkens, M. F. P., Bouwman, A., Jongman, B., ... & Ward, P. J. (2016). Global drivers of future river flood risk. *Nature Climate Change*, 6(4), 381–385. https://doi.org/10.1038/nclimate2893

World Bank (2024) *Subnational Poverty and Inequality Database (SPID)*. Poverty and Inequality Platform (PIP). Available at: https://pipmaps.worldbank.org/en/data/datatopics/poverty-portal/poverty-interactivemap (Accessed: 11 August 2025).

World Health Organization (WHO). (2025). *Pakistan floods emergency situation report 2025.*

WorldPop. (2022). Global high-resolution population denominators project. University of Southampton. https://www.worldpop.org/

Zack, G. W., Rogers, W. E., & Latt, S. A. (1977). Automatic measurement of sister chromatid exchange frequency. *Journal of Histochemistry & Cytochemistry, 25*(7), 741–753. https://doi.org/10.1177/25.7.70454 *(Note: I corrected the page range based on the official DOI record, as the numbers provided in your text were slightly off.)*